High frequency, continuous measurements reveal strong diel and seasonal cycling of pCO_2 and CO_2 flux in a mesohaline reach of the Chesapeake Bay

A. Whitman Miller[1*], Jim R. Muirhead[1], Amanda C. Reynolds[1], Mark S. Minton[1] and Karl J. Klug[1]

[1]Smithsonian Environmental Research Center, Edgewater, MD USA

Corresponding author: A. Whitman Miller (millerw@si.edu)

†Additional author notes should be indicated with symbols (current addresses, for example).

Key Points:

- Automated pCO_2 measurements capture daily cycles and anomalous events in estuaries where pCO_2 changes rapidly and across a wide range.
- Rhode River is net autotrophic (Dec-May), net heterotrophic (Jun-Nov), NEP is near balanced annually, but can reverse status during a single day.
- Year-round continuous measurements reveal that pCO_2 and CO_2 flux are mediated by temperature effects on biological activity and are inverse to the physical solubility of CO_2.

ABSTRACT

We estimated hourly air-water gas transfer velocities (k_{600}) for carbon dioxide in the Rhode River, a mesohaline subestuary of the Chesapeake Bay. Gas transfer velocities were calculated from estuary-specific parameterizations developed explicitly for shallow, microtidal estuaries in the Mid-Atlantic region of the United States, using standardized wind speed measurements. Combining the gas transfer velocity with continuous measurements of pCO_2 in the water and in the overlying atmosphere, we determined the direction and magnitude of CO_2 flux at hourly intervals across a 3 yr record (01 July 2018 to 01 July 2021). Continuous year-round measurements enabled us to document strong seasonal cycling whereby the Rhode River is primarily autotrophic during cold-water months (Dec–May), and largely net heterotrophic in warm-water months (Jun–Nov). Although there is inter-annual variability in CO_2 flux in the Rhode River, the annual mean condition is near carbon neutral. Measurement at high temporal resolution across multiple years revealed that CO_2 flux and apparent trophic status can reverse during a single 24 hr period. pCO_2 and CO_2 flux are mediated by temperature effects on biological activity and are inverse to temperature-dependent physical solubility of CO_2 in water. Biological/biogeochemical carbon fixation and mineralization are rapid and extensive, so sufficient sampling frequency is crucial to capture unbiased extremes and central tendencies of these estuarine ecosystems.

1. Introduction

Understanding the air–sea exchange of gases and establishing methodologies for accurate measurements has been a decades-long focus of atmospheric scientists, oceanographers, and biogeochemists seeking to understand interactions between oceans and the atmosphere and how these interactions contribute to the global carbon cycle (Broecker et al., 1979; Wanninkhof, 1992, 2013). Coastal oceans and estuaries are ecosystems of interest for understanding the complex nature and contribution of the land–sea interface to lateral mass transport of carbon (Abril & Borges, 2005; Cai & Wang, 1998; Frankignoulle et al., 1998; Song et al., 2023) but also with respect to the role these ecosystems play as both atmospheric CO_2 sources and sinks (Abril & Borges, 2005; Chen et al., 2020; Dai et al., 2022; Jiang et al., 2008). The exchange of carbon dioxide, methane, and other greenhouse gases (GHGs)between Earth's atmosphere and inland waters, estuaries, coastal oceans are well-documented but not fully quantified (Abril & Borges,

2005; Cai, 2011; Laruelle et al., 2017; Raymond & Cole, 2001; Raymond et al., 2013; Van Dam et al., 2019). CO_2 evasion from estuaries alone has been estimated at 15–17% of the total CO_2 input from oceans to the atmosphere (Chen et al., 2020; Laruelle et al., 2017), indicating the regional and global significance of estuaries (Bauer et al., 2013; Frankignoulle et al., 1998; Jiang et al., 2008). Yet, there is still great uncertainty surrounding the true net contributions of coastal oceans, estuaries, and inland water bodies to the atmospheric loading of GHGs (Borges, 2005; Chen et al., 2020; Herrmann et al., 2020; Joesoef et al., 2015; Laruelle et al., 2017; Raymond et al., 2013; Van Dam et al., 2019).

To better understand the effects of estuaries on atmospheric GHG exchange and accumulation, it is imperative that we understand their capacity and function as carbon sources and sinks and ultimately how estuaries factor into the planet's overall global carbon budget (Herrmann et al., 2020; Laruelle et al., 2017; Van Dam et al., 2019). Many attempts to characterize CO_2 flux in estuaries and nearshore oceans (Chen et al., 2013; Herrmann et al., 2020; Rosentreter et al. 2021) have relied on direct measurements using floating domes, tracer gases or, more recently, eddy covariance methods (Laruelle et al, 2017; Van Dam et al., 2019). Because flux measurements are time intensive, they tend to be temporally and spatially limited (Herrmann et al., 2020; Klaus & Vachon, 2020). Using direct flux measurements to derive accurate gas transfer velocity constants (K_o, the velocity of gas crossing the air-water boundary) enables models to be parameterized to estimate K_o and compute gas flux. Thus, correlative models that incorporate simultaneous environmental measurements such as wind and/or water velocity, factors that affect turbulence at the air-water interface and promote gas exchange, have aided in the widespread accumulation of gas flux estimates (Raymond & Cole, 2001; Van Dam et al., 2019; Wanninkhof, 2014). Gas transfer velocity constant models vary according to the habitat/system being observed and chemical, physical, and biological factors present in each (e.g., lakes, rivers/streams, estuaries, and oceans; Herrmann et al., 2020; Ho et al., 2016; Raymond & Cole, 2001; Van Dam et al., 2019; Wanninkhof, 1992). To reduce uncertainty of computed gas fluxes, it is critical that the appropriate K_o models are matched to a targeted ecosystem.

Coastal oceans and estuaries are exceptionally complex, frequently characterized by their relative shallowness and how their freshwater inputs (riverine, surface, and groundwater) mix with salt

water (Chen et al., 2020). High nutrient and pollutant loading, due to urbanization and eutrophication by humans, also have important effects on estuaries and coastal oceans (Freeman et al., 2019). High spatial and temporal variability are hallmarks of estuaries.

Here we present a 3 year data set that combines high frequency (1 min interval) measurements of dissolved and atmospheric CO_2 with co-located and continuous measurements of salinity, water temperature, tidal cycling, and wind velocity, recorded at the Smithsonian Environmental Research Center (SERC) dock, in the Rhode River, Maryland. To estimate hourly, daily, seasonal, and annual CO_2 flux rates, we applied a CO_2 gas velocity constant model developed by Van Dam et al. (2019) for the New River, North Carolina. This model is expressly designed for application to shallow, well-mixed, microtidal estuaries located in the Mid-Atlantic coast of the United States.

2. Methods

2.1 Study Location

The Rhode River is a tributary and subestuary of the Chesapeake Bay, a drowned river valley, coastal plain estuary (Fig. 1). The Rhode River has been studied extensively by SERC staff and colleagues for over 4 decades: nutrient chemistry (Jordan & Correll, 1991; Jordan et al., 1991), phytoplankton ecology (Gallegos et al., 2010), color dissolved organic matter distribution (Tzortziou et al., 2008; Tzortziou et al., 2011), and more recently, modeling of dissolved organic carbon (DOC) input from freshwater and tidal marsh sources (Clark et al., 2020). Located on the Bay's northwestern shore (38º52'N, 76º32'W), the Rhode River is bounded at its head by Muddy Creek and at its mouth by the mainstem of the Chesapeake Bay. The Rhode River is a shallow (mean depth = 2 m, max depth = 4.1 m), mesohaline (0 to 18 ppt), well-mixed, eutrophic tributary with a length of approximately 5 km; its surface area is approximately 5 km^2 with a shoreline perimeter of 39 km (Breitburg et al., 2008; Clark et al., 2018). A 0.21 km^2 tidal marsh (Kirkpatrick Marsh) fringes the estuary at the mouth of Muddy Creek (Fig. 1). Tides are semi-diurnal with a mean amplitude of approximately 30 cm, but water height can be strongly affected by wind and weather events. Muddy Creek is the main freshwater source of the Rhode River and has a maximum flow rate of 10.42 $m^3 \cdot s^{-1}$ and mean flow rate 0.18 $m^3 \cdot s^{-1}$ (mean flow = 15,552 $m^3 \cdot d^{-1}$; Clark et al., 2020; Clark et al., 2018; Jordan et al., 1986). The mean daily volume of

freshwater inflow from Muddy Creek is approximately 0.5% of the mean daily tidal exchange volume, based on the Rhode River's area and mean tidal amplitude. In the absence of measurements of the pH or pCO_2 of the freshwater entering the Rhode River from Muddy Creek or other lesser freshwater inputs to the estuary, we are unable to report these pCO_2 or pH values. However, given the exceedingly small overall volume of freshwater input to the Rhode River from its surrounding watershed, it is not considered a river-dominated estuary so is not expected to be substantially influenced by the chemical characteristics of this input. This is not to say there is no freshwater influence, only that such influences are likely quite local when mixing with far larger volumes of water from the Chesapeake Bay and therefore beyond the resolution of this study.

Although the Rhode River is a model ecosystem that has been studied intensively for several decades across many dimensions (Clark et al. 2018; Correll et al., 1992; Gallegos et al., 1992; Jordan et al. 1991; Rose et al. 2019), no work to date has expressly characterized the nature and dynamics of CO_2 flux between the river and the atmosphere.

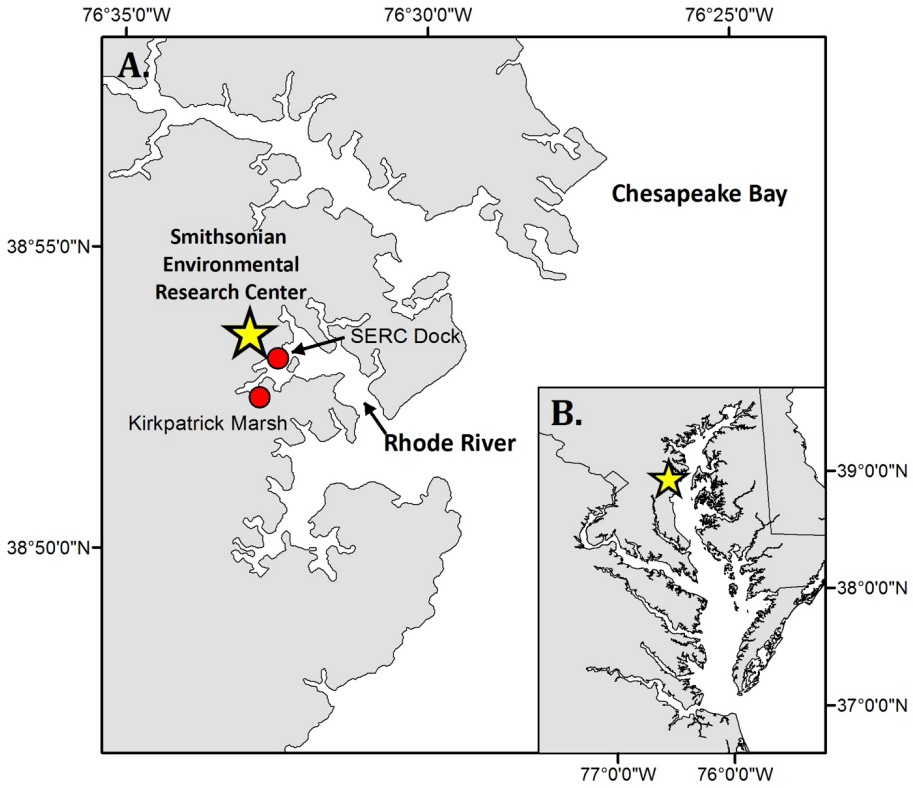

Fig. 1. Location of study site on the Rhode River, Edgewater MD (A), as situated in the Chesapeake Bay (B). All pCO_2 and related water quality values reported were measured from the SERC dock, that extends approximately 75 m from shore on Rhode River. Red circles indicate location of dock and a tidal creek that drains the Kirkpatrick saltmarsh (marsh area = 0.21 km^2, 1 km up estuary from the dock).

2.2 *In Situ* Measurements, Calculated Parameters and Quantities

Continuous, automated environmental measurements were made in and above the Rhode River during a 3 year period between 01 July 2018 and 01 July 2021. The purpose of these

measurements was to document fluctuations in aqueous pCO_2 on a fine time scale, from which CO_2 flux between the water and atmosphere could be calculated.

2.2.1 Aqueous CO_2 (pCO_{2water})

To measure the CO_2 gradient ($\Delta C = pCO_{2water} - pCO_{2air}$) across the Rhode River surface waters and its overlying atmosphere, measurements of pCO_2 were made with a non-dispersive infrared (NDIR) detector. In the case of dissolved gas measurements, water was equilibrated continuously with a spherical falling film equilibrator (Miller et al. 2019). Water from 1 m below the water's surface was pumped and dispersed continuously over a 25.4 cm diameter sphere. The falling film created on the sphere generates a gas exchange surface which forces CO_2 in the equilibrator headspace into equilibrium with the water's CO_2 content (i.e. mole fraction = xCO_2 (μmol/mol). Water exits the equilibrator via an airtight drain that prevents headspace contamination from surrounding atmospheric air. Headspace gas circulates continuously in a closed loop through the equilibrator, water trap and gas dehumidifier, past the NDIR, and back into the equilibrator. Experimental observations concluded that spherical falling film equilibrators achieve 99% equilibration of CO_2 within 10–15 mins, depending on whether step changes are from low to high or high to low; details of the operation and performance of the falling film equilibrator are described in Miller et al. (2019). Measurements were made at 1 min intervals at a pressure equal to the ambient barometric pressure.

Measured raw CO_2 mole fractions (μmol/mol) were converted to partial pressures (μatm) using equation 1. Minute-over-minute values were rounded down to the nearest hour and averaged to provide hourly means. The mole fractions were then evaluated with corresponding water temperature and salinity measurements following the methodology of Zeebe and Wolf-Gladrow (2001) where saturation vapor pressure of water is calculated according to Weiss and Price (1980) to determine pCO_{2water}.

$$pCO_{2water} = xCO_2 \cdot (p - pH_2O) \quad (1)$$

where

pCO_2 = partial pressure of CO_2 of water (μatm)

xCO_2 = mole fraction of CO_2 in water (μmol/mol)

170 p = total pressure = 1 atm
171 pH_2O = saturation vapor pressure of water (μatm)
172
173 2.2.2 Atmospheric CO_2
174 Every six hours, the sample gas stream was automatically diverted with programmed solenoid
175 control valves from the equilibrator to an atmospheric port located approximately 5 m above the
176 pier deck. During atmospheric sampling, 15 1-min interval measurements were made. To
177 account for inaccuracies during the transition period from equilibrator to atmospheric sampling,
178 the final eight measurements were averaged and the first seven were discarded. Similarly, the
179 first 30 measurements following switchover from atmospheric port to equilibrator were
180 discarded, to ensure measurements were fully equilibrated with water. For these atmospheric
181 measurements, the contribution of the vapor pressure of water to the total atmospheric pressure
182 of the open-air environment was considered negligible (i.e. $pH_2O = 0$ and $p = 1$), such that
183 $pCO_{2atm} = xCO_{2atm.}$ As such, any potential differences are expected to fall well within the
184 measurement accuracy of the instrument (see below).
185
186 One advantage to using a shared NDIR sensor for aquatic and atmospheric samples is that any
187 minor effects of instrument drift will be reflected in both data streams, as opposed to two sensors
188 that drift independently of one another. Likewise, significant and sustained deviation from
189 typical local atmospheric variability will be captured during atmospheric sampling and can signal
190 the need for recalibration and assist with QA/QC of corresponding data from both streams. A
191 disadvantage of using a common sensor for both dissolved and atmospheric CO_2 measurements
192 is that it results in a mismatch in sampling frequency of the two. With this limitation in mind, we
193 chose a higher sampling frequency for aquatic measurements to better describe the inherently
194 higher variability in dissolved CO_2 in water vs. that in the atmosphere (Fig. 2).

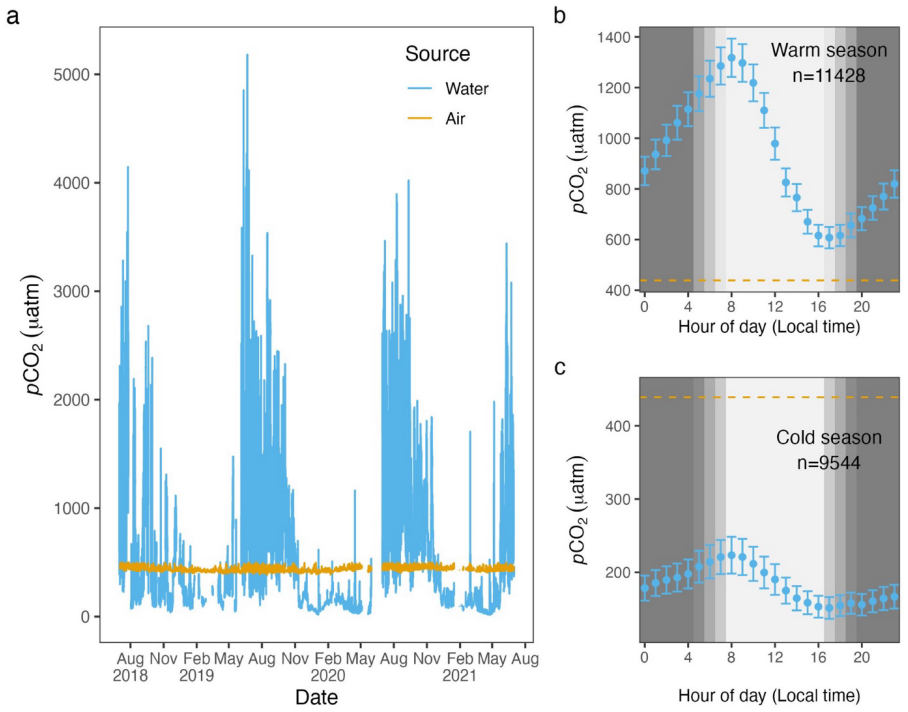

Fig. 2. Hourly pCO_{2water} (blue) and pCO_{2air} (goldenrod) values from 01 July 2018 to 01 July 2021 (panel a). The air-water CO_2 gradient, $\Delta C = pCO_{2water} - pCO_{2air}$ describes the directionality of gas diffusion. Negative ΔC values (pCO_{2water} values falling below goldenrod demarcation) represent gas movement from air to water and vice versa. Panels b and c depict mean pCO_{2water} values (95% CI) for each hour of the day for warm and cold seasons, with the dashed lines equal to the mean 3 yr value of pCO_{2air}.

Given the 3 yr time series and strong diel cycling of pCO_{2water} (and dissolved oxygen (DO), see Figs. S1 and S2) in the Rhode River, we chose to aggregate aqueous minute-over-minute measurements to mean hourly averages. Owing to the relative lack of short-term variability in local atmospheric CO_2 concentrations (Fig. 2), we used linear interpolation to impute atmospheric CO_2 concentrations during hours in between actual readings (6 hr gaps between atmospheric measurements), which we assumed to be more realistic and reliable than Last Observation Carried Forward (LOCF) methods, where the last observation is repeated for all gaps until the next measurement is encountered, a method that has fallen out of favor, especially

211 for environmental time series data (Lachin, 2016). To determine if any inadvertent bias was
212 introduced by linear interpolation procedure, summary statistics of actual atmospheric readings
213 and actual readings + imputed CO_2 values were compared statistically. This approach enabled us
214 to take advantage of >25,000 time points throughout the 3 yr period of observation, providing
215 hourly resolution. Mean pCO_{2air} = 437 ± 20.0 µatm (Table 1), variability that falls well within
216 manufacturer's specifications (see section 2.2.4).
217
218 2.2.3 CO_2 gradient (ΔC)
219 ΔC was determined by subtraction, $pCO_{2water} - pCO_{2air}$, where positive ΔC values correspond to
220 higher CO_2 concentrations in the water, tending toward movement from water to air (outgassing
221 or evasion, where Rhode River = CO_2 source), and negative values that signal CO_2 transport
222 from air to water (dissolution, where Rhode River = CO_2 sink). Figure 2 shows pCO_{2water} and
223 pCO_{2air} plotted on an hourly basis for the 3 yr period beginning 01 July 2018 and ending 01 July
224 2021. Across this period, ΔC was predominantly negative during cold months and predominantly
225 positive during warm months when pCO_{2water} tended to reach the highest values of the year, but
226 ΔC sometimes reversed sign due to occasional extreme day-time photosynthetic drawdown of
227 CO_2 (Fig. 2).
228
229 2.2.4 Accuracy of CO_2 measurements
230 Estimated accuracy of the spherical falling film equilibrator and NDIR sensor (SenseAir K30,
231 https://senseair.com/) combination were experimentally determined in the lab and found to
232 measure water equilibrated with known gas concentrations to be within the ±1% uncertainty
233 limits of the of certified standard gas mixtures used, and well within the published accuracy
234 specification of the SenseAir K30 (i.e., ± 30 ppmv ± 3% of instrument reading). Experimental
235 analysis by Martin et al. (2017) report even higher accuracy when relative humidity and
236 atmospheric pressure are controlled for. Details on performance of the spherical falling film
237 equilibrator, such as accuracy, precision, and time constants can be found in Miller et al. (2019).
238 Although SenseAir offers automated calibration via long term comparisons to atmospheric
239 readings, this feature was deactivated. The K30 NDIR was periodically validated using standard
240 zero CO_2 (nitrogen) and standard certified span gases at intervals of one to two months during
241 the study period. Although the K30 was never observed to drift beyond its factory specifications,

the sensor was occasionally re-calibrated in the lab, and measured values were accepted without adjustment.

CO_2 measurements were downloaded to a database at approximately two-week intervals during the observation period. Data were graphed and reviewed visually, in combination with twice weekly observations of equilibrator function recorded in an accompanying notebook. Anomalous data were flagged and excluded from data analysis (e.g., flooding or clogging events that interrupted proper equilibration.)

2.3 Co-located water quality and atmospheric measurements

This water quality station at the SERC dock is a long-term node of the Maryland Department of Natural Resources "Eyes on the Bay" Chesapeake Bay tidal water monitoring program, and has been operated by the SERC since 1986. Water quality and atmospheric data are maintained by the MarineGEO Upper Chesapeake Bay Observatory and can be accessed online (Benson et al., 2023). A YSI EXO2 sonde was positioned 1 m below the water's surface and in proximity (~2.5 m distance) to the submerged water pump that fed the pCO_2 equilibrator. Sonde measurements were made at 6 minute intervals and aggregated to 1 hr averages. The published accuracy specifications for the YSI sonde are as follows: temperature: ±0.01 ºC (-5º to 35º C); salinity: ±1% of reading or 0.1 ppt (0–70 ppt); dissolved oxygen: ±0.1 mg/L or 1% of reading (0 to 20 mg/L). Discrete measurements of temperature and salinity were made with a handheld YSI Professional Plus 2030 with Quattro Cable instrument, with the following specifications: temperature: ±0.02 ºC (-5º to 70º C); salinity: ±1% of reading or 0.1 ppt (0–70 ppt); dissolved oxygen: ±0.2 mg/L or 2% of reading (0 to 20 mg/L). Equilibrator temperature was measured with a probe (EDS model OW-TEMP-B3-12xA) accurate to ±0.5 ºC (-10º to 85 ºC). Discrete measurements were routinely compared with the sonde to corroborate measurement agreement. Wind speed measurements were made using a sonic anemometer (Vaisala WXT-520 weather transmitter) mounted 7 m above the mean low tide height of the water and located directly above the pCO_2 equilibrator.

2.4 Data Processing

Data included in this study span 01 Jul 2018 to 01 Jul 2021.

2.4.1 Gas-specific solubility

To determine the purely physical effects of temperature and salinity on CO_2 solubility, gas-specific solubility values K_0 (mmol · m^{-3} · µatm^{-1}) were calculated across the 3 yr observation period using water temperature and salinity measurements in combination with pCO_{2water} values, according to Weiss and Price (1980) at 1 hour intervals.

2.4.2 Gas transfer velocity estimation (k)

Given the similarities between the Rhode River and New River estuaries (e.g., shallow, microtidal estuaries with slow water velocity and strong diel cycles in pCO_2 and DO), we chose to parameterize gas transfer velocity k (cm · h^{-1}) standardized to the unitless Schmidt number 600 (k_{600}) according to the estuary-specific k parameterization model developed by Van Dam et al. (2019). Van Dam et al. (2019) determined that k correlated with wind speed differently during daytime versus nighttime hours (linear vs. parabolic relationships). Wind speed data were collected during the 3 yr period from a sonic anemometer located on the SERC dock directly above the equilibration system and approximately 7 m above the water's surface at mean low tide height. For the analysis, windspeeds were standardized for a height of 10 m following a power-law relationship, $U_{10} = U_7 * (10/7)^{0.15}$ (Saucier, 2003). Following Van Dam et al., wind speed data were binned to 1.5 m s^{-1} intervals for day and night readings and raw values replaced by the mean wind speed for each bin. The median binned windspeed over the Rhode River was 2.2 m s^{-1}, regardless of time of day or season. Recorded windspeeds never exceeded 10m s^{-1} and were dominated by much lower values (Fig. S1). Unlike the New River Estuary, the Rhode River's windspeed profile does not differ much between day and night, nor across season. For this reason, we chose to use the most conservative k_{600} formulation from Van Dam et al (2019), that combines day and night winds to estimate k_{600}.

Wind speed was used to parameterize k_{600} as follows:

$$k_{600} = 1.5 * U_{10} + 4.2 \quad (2)$$

where U_{10} = mean of binned wind speed at 10 m above the water's surface (m · s^{-1}).

304 2.4.3 CO_2 flux

305 Using continuous, parallel 3 yr records (01 July 2018 to 01 July 2021) of dissolved and
306 atmospheric pCO_2, water temperature, salinity, and wind speed (at standard 10m height, U_{10}),
307 CO_2 flux was derived according to the equation:
308
309 $$CO_2 \text{ flux} = k_{600} \cdot K_0 \cdot \Delta C \cdot (600 / Sc)^{-0.5} \quad (3)$$
310 where
311 CO_2 flux = the rate and direction of CO_2 mass moving between water and gas phases
312 ($mmol \cdot m^{-2} \cdot hr^{-1}$)
313 k_{600} = gas transfer velocity ($cm \cdot hr^{-1}$), normalized to a common Schmidt number
314 ($Sc = 600$)
315 K_0 = gas-specific solubility for CO_2 ($mmol \cdot m^{-3} \cdot \mu atm^{-1}$)
316 ΔC = air-water concentration gradient (μatm)
317 Sc = Schmidt number
318
319 Note: CO_2 flux calculations require conversion from traditional k_{600} units ($cm \cdot hr^{-1}$) to ($m \cdot hr^{-1}$)
320 from ΔC units (μatm) to (atm) prior to calculation.
321
322 2.4.4 Day/Night Designation
323 To differentiate daytime from nighttime hours, we used the position of the measurements
324 (latitude) in the Rhode River, combined with the local date and time. This approach enabled us to
325 uniformly designate various environmental measurements as happening during the day or night
326 (R package "LakeMetabolizer", Winslow et al., 2016).
327
328 2.4.5 Seasonality
329 We chose to break the year into two 6 month periods based seasonal water temperature shifts,
330 designating June–November as "warm-water months" when water temperatures averaged 23.2 ±
331 6.90 °C. (mean ± 1 sd) and December–May as "cold-water months", 10.9 ± 5.66 °C (Figs. S1and
332 S2).
333
334

335 2.4.6 Effect size

336 Owing to the large number of observations available for comparison in this study, the likelihood
337 of finding statistically significant results is quite high. Whether such statistical results by
338 themselves connote practical and informative differences can be difficult to discern. Effect sizes
339 (Omega-squared, ω^2) were calculated according to two-factor ANOVAs where independent
340 variables were investigated by season (cold-water vs. warm-water season), day/night period and
341 the interaction of season and day/night. The independent variables compared were: K_0, CO_2 flux,
342 ΔpCO_2, k_{600}, pCO_{2air}, pCO_{2water}, and wind speed. To account for temporal autocorrelation and
343 lack of independence of observations that are typical of environmental time series data, we
344 corrected for overinflation in the residual mean square used in the effect size calculations by
345 removing the autocorrelation present within residuals, leaving the white-noise component as the
346 unbiased estimate of residual variability (Cochrane-Orcutt procedure, R package "orcutt", Spada
347 et al., 2018).
348
349 **3. Results and Discussion**
350 3.1 Daily and Seasonal Cycling of pCO_2
351 Hourly averaged measurements of pCO_{2water} in the Rhode River across three years revealed
352 strong diel and seasonal cycling (Fig. 2). Mean and maximum pCO_{2water} were significantly higher
353 in warm-water vs. cold-water months (Table 1). During warm-water months (Jun–Nov) daily
354 oscillations of pCO_2 frequently transit from far above to below ambient atmospheric conditions
355 over the course of the day, only to reverse direction (from low to high) during the nighttime
356 hours (Fig. 2). During the summer, pCO_{2water} levels sometimes shifted by as much as 4500 µatm
357 in both directions during a single 24 hr period (Fig. 2). This pattern is consistent with
358 biologically driven cycling whereby very high early morning pCO_{2water} conditions are depleted
359 by net photosynthetic activity (inorganic carbon fixation) over the course of the day, but high
360 pCO_{2water} is restored by respiration in the benthos and water column at night (Song et al. 2023).
361 Comparing dissolved oxygen (DO) over the same period, similar harmonic cycling is observed,
362 but maximums and minimums of pCO_2 and DO were inversely related (Fig. S1), hallmarks of a
363 production/respiration driven system (Herrmann et al., 2020; Van Dam et al., 2019).
364

Table 1. Descriptive statistics comparing seasonality of pCO_2, CO_2 flux and associated parameters in cold-water (Dec–May) and warm-water seasons (Jun–Nov).

Season	Time Period	Variable	Units	N	Mean	Min	Max	SD
overall	**-**	**CO_2 flux**	**mmol · m^{-2} · hr^{-1}**	**20971**	**-0.09**	**-4.89**	**11.18**	**1.823**
cold	day	CO_2 flux	mmol · m^{-2} · hr^{-1}	4494	-1.39	-4.89	8.26	1.134
cold	night	CO_2 flux	mmol · m^{-2} · hr^{-1}	5050	-1.39	-4.66	5.24	0.927
warm	day	CO_2 flux	mmol · m^{-2} · hr^{-1}	6007	1.18	-3.95	11.18	1.731
warm	night	CO_2 flux	mmol · m^{-2} · hr^{-1}	5421	0.78	-3.97	8.05	1.467
overall	**-**	**K_0**	**mmol · m^{-3} · µatm^{-1}**	**20971**	**0.04**	**0.03**	**0.07**	**0.011**
cold	day	K_0	mmol · m^{-3} · µatm^{-1}	4494	0.05	0.03	0.07	0.009
cold	night	K_0	mmol · m^{-3} · µatm^{-1}	5050	0.05	0.03	0.07	0.008
warm	day	K_0	mmol · m^{-3} · µatm^{-1}	6007	0.03	0.03	0.06	0.007
warm	night	K_0	mmol · m^{-3} · µatm^{-1}	5421	0.04	0.03	0.07	0.008
overall	**-**	**k_{600}**	**cm · hr^{-1}**	**20971**	**7.86**	**5.57**	**18.36**	**2.047**
cold	day	k_{600}	cm · hr^{-1}	4494	8.71	5.57	16.33	2.251
cold	night	k_{600}	cm · hr^{-1}	5050	7.74	5.57	18.36	2.081
warm	day	k_{600}	cm · hr^{-1}	6007	7.92	5.57	18.36	1.868
warm	night	k_{600}	cm · hr^{-1}	5421	7.20	5.57	18.36	1.751
overall	**-**	**ΔC**	**µatm**	**20971**	**154**	**-436**	**4750**	**645.8**
cold	day	ΔC	µatm	4494	-239	-436	1553	220.9
cold	night	ΔC	µatm	5050	-256	-434	1204	164.2
warm	day	ΔC	µatm	6007	570	-399	4750	745.5
overall	**-**	**pCO_{2air}**	**µatm**	**20971**	**437**	**387**	**500**	**20.0**
cold	day	pCO_{2air}	µatm	4494	430	390	497	16.0
cold	night	pCO_{2air}	µatm	5050	432	387	499	17.8
warm	day	pCO_{2air}	µatm	6007	439	390	499	20.7
warm	night	pCO_{2air}	µatm	5421	443	387	500	21.5
overall	**-**	**pCO_{2water}**	**µatm**	**20971**	**591**	**15**	**5182**	**651.8**
cold	day	pCO_{2water}	µatm	4494	191	15	1982	220.9
cold	night	pCO_{2water}	µatm	5050	176	17	1638	163.9
warm	day	pCO_{2water}	µatm	6007	1009	47	5182	752.6
warm	night	pCO_{2water}	µatm	5421	844	38	4855	632.2
overall	**-**	**wind speed**	**m · s^{-1}**	**20971**	**2.4**	**0.1**	**9.8**	**1.42**
cold	day	wind speed	m · s^{-1}	4494	3.1	0.3	8.9	1.53
cold	night	wind speed	m · s^{-1}	5050	2.4	0.3	9.1	1.45
warm	day	wind speed	m · s^{-1}	6007	2.5	0.1	9.8	1.28
warm	night	wind speed	m · s^{-1}	5421	2.0	0.1	9.1	1.23

On the seasonal timescale, pCO_2 was consistently lowest and DO highest during cold-water months of the year (Dec–May; Fig. S1). Importantly, for both gases the temporal variability (diel

371 cycling; Fig. S2) was most constrained during cold-water months across years, strongly
372 suggesting that carbon fixation exceeds respiration for prolonged periods (weeks to months). In
373 contrast, during warm-water months (Jun–Nov), photosynthesis/carbon fixation and respiration
374 are more evenly balanced, compensating one another over 24 hr periods (i.e., respiration >
375 productivity at night and productivity > respiration during daylight hours; Fig. 2).
376
377 3.2 Air-water concentration gradient = ΔC (µatm)
378 When hourly pCO_{2water} and pCO_{2air} values (composed of 4 hourly measurements and 20
379 interpolated values per day) were plotted across the three years of observation, the diel and
380 seasonal cycles of pCO_{2water} are evident. As expected, atmospheric concentrations of CO_2
381 remained relatively constant compared with aqueous loads. When the mean raw pCO_{2air}
382 measurements (mean = 435.1, 95% CI [434.4, 435.7]) were compared with raw pCO_{2air}
383 measurements + imputed estimates (mean = 435.4, 95% CI [435.2, 435.7]) no statistical
384 difference was observed, indicating that no substantial bias was introduced by linear
385 interpolation of atmospheric measurements.
386
387 Although nearshore atmospheric CO_2 concentrations are expected to vary more than those in
388 isolated well-mixed atmosphere (e.g., at the Mona Loa Observatory), annual mean values were
389 consistent and within the published uncertainty of the K30 NDIR sensor, when compared with
390 global measurements conducted at Mona Loa (Thoning et al., 2023). Local perturbations (e.g.,
391 effects of terrestrial photosynthetic drawdown when wind is absent) were apparent in
392 measurements (Fig. 2) but there were no instances when the measured local atmospheric values
393 were suspiciously high or low for days on end, as compared with expected global mean
394 atmospheric values for the time period (i.e., 408–416 ppmv; https://www.co2.earth/annual-co2,
395 Thoning et al., 2023). This lack of sustained anomalous deviation served as additional
396 confirmation that the K30 was functioning properly and had not drifted outside its calibration
397 range. Importantly, given the extreme diel cycling and seasonal variability of the Rhode River's
398 pCO_{2water}, the absolute accuracy necessary for determining year-over-year changes in
399 atmospheric or ocean pCO_2 is not a requirement for these CO_2 flux calculations which rely on
400 relative differences between water and atmospheric measurements.
401

Hourly air-water concentration gradient values = ΔC (μatm) were calculated and plotted across the three years of study (Fig. 2). During warm months, pCO_{2water} routinely shifts from supersaturated to sub-atmospheric and back again, over the course of 24 hours (e.g., between >2000 μatm and <410 μatm on a single day). These large daily swings in pCO_{2water} produced concomitant directional reversals of ΔC ($pCO2_{water} - pCO_{2air}$), which result in longer term averaged gradients (e.g., multi-day, multi-week averages) near zero (Fig. 2). In contrast, most of the time during cold-water months is spent in a state of sub-atmospheric pCO_{2water} (under-saturation with respect to overlying atmosphere), resulting in ΔC values that are negative and which promote movement of CO_2 from the atmosphere into the water.

3.3 Gas-specific solubility (K_0)

To account for the physical effects of temperature and salinity on the solubility of CO_2 in estuarine water, K_0 was calculated by methods of Weiss and Price (1980). K_0 varied strongly across seasons over the 3 yr observation period. The maximum annual range = 0.027 to 0.071 $mmol \cdot m^{-3} \cdot \mu atm^{-1}$; mean cold-water months = 0.051 and mean warm-water months = 0.035 $mmol \cdot m^{-3} \cdot \mu atm^{-1}$, confirming that CO_2 was most soluble during winter and least soluble in summer (Fig. 3). This is inverse to observed dissolved CO_2 values: pCO_{2water} was lowest and least variable during winter and highest and most variable during summer (Fig. 2, Table 1) suggesting that solubility, in and of itself, plays only a minor and non-limiting role in pCO_{2water} in the Rhode River. Effect size (ω^2) estimates indicated that the greatest proportion of variability in K_0 was associated with season, vs. day/night or the interaction of the two (Table 2).

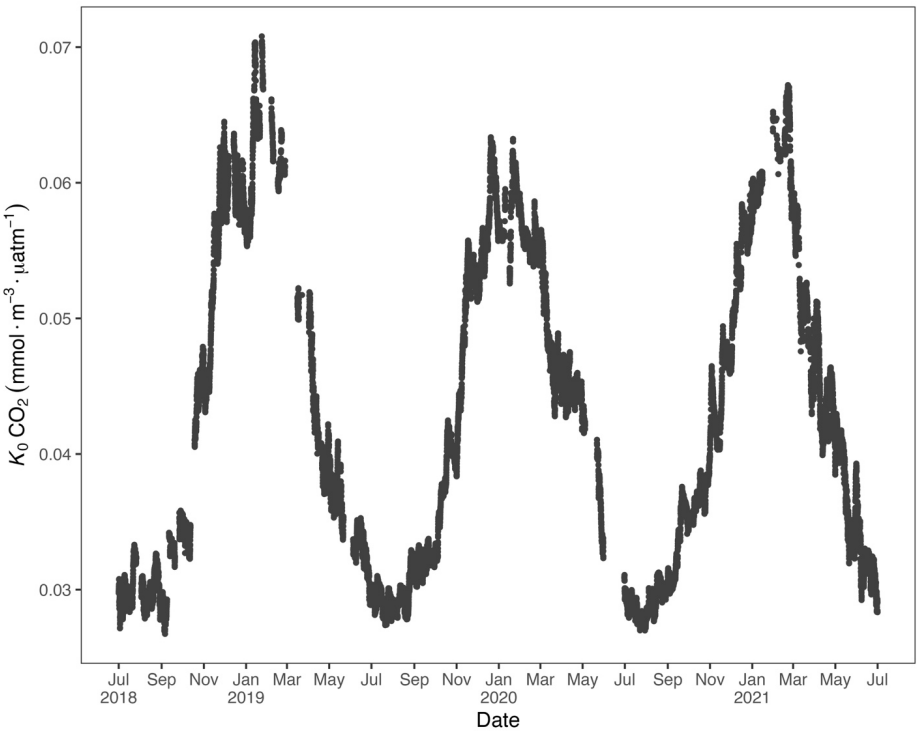

Fig. 3. Gas-specific solubility (K_0) for CO_2 based on water temperature and salinity. Units are mmol m^{-3} µatm^{-1} in the Rhode River (01 Jul 2018 to 01 Jul 2021).

Table 2. Contrast effect sizes based on two-factor ANOVA where independent variables were compared by season (cold-water season = Dec–May vs warm-water season = Jun–Nov), day/night period and the interaction of the two. ω^2 is a measure of effect size, estimating the proportion of total variance explained by each parameter. Effect sizes were corrected for inherent temporal autocorrelation using the Cochrane-Orcutt procedure (Spada et al., 2018).

Variable	Factor	Effect Size (ω^2)
K_0	Season	0.0300
K_0	Day/Night	0.000575
K_0	Season:Day/Night	0.0000140
CO_2 flux	Season	0.415
CO_2 flux	Day/Night	0.00295
CO_2 flux	Season:Day/Night	0.00301
ΔC	Season	0.310
ΔC	Day/Night	0.00501
ΔC	Season:Day/Night	0.00333
k_{600}	Season	0.00164
k_{600}	Day/Night	0.00269
k_{600}	Season:Day/Night	0.0000549
pCO_{2air}	Season	0.000137
pCO_{2air}	Day/Night	0.0000134
pCO_{2air}	Season:Day/Night	0.00000137
$pCO_{2\ water}$	Season	0.188
$pCO_{2\ water}$	Day/Night	0.00275
$pCO_{2\ water}$	Season:Day/Night	0.00191
wind speed	Season	0.00711
wind speed	Day/Night	0.0186
wind speed	Season:Day/Night	0.000182

3.4 Temperature/Biology ratio

To independently parse the magnitude of the physical versus biological forcing of pCO_{2water}, we normalized values to mean water temperature and estimated the Takahashi's Temperature/Biology ratio (Takahashi et al., 2002) to compare the influence of temperature and biological activities on pCO_{2water}. Across the 3-year period, we found that the predominant driver of pCO_{2water} in the Rhode River was biological activity, accounting for nearly 4 times more forcing than the physical effects of water temperature on CO_2 solubility (Table 3). These patterns demonstrate the outsized role that biological processes play in shaping pCO_{2water} in nearshore marine and estuarine ecosystems (Dai et al., 2022; Van Dam et al., 2019).

Formatted: Subscript

Deleted: Across the 3 year period, we found that just 26.0 ± 4.0% (mean ± SD) of forcing was attributable to the effect of temperature on solubility, confirming that the predominant driver of pCO_{2water} in the Rhode River is indeed biological activity (75%, Table 3).

Formatted: Subscript

Table 3. Takahashi Temperature/Biology Ratio (Eq. 5a From Takahashi et al. 2002).

Year	N	ΔpCO_2_bio	ΔpCO_2_temp	T/B ratio
2018	4416	3193.0	765.8	0.240
2019	8760	3669.8	1019.6	0.278
2020	8784	2772.1	846.0	0.305
2021	4345	2356.1	507.2	0.215
Overall	26305	3701.5	926.4	0.250

3.5 Gas transfer velocity (k_{600})

Gas transfer velocity is affected by both mass transfer from molecular diffusion driven by ΔC (i.e. CO_2 gradient between water and atmosphere) and momentum transfer linked to external environmental forces that enhance turbulence at the air-water boundary layer (Ho et al., 2016; Raymond & Cole, 2001; Van Dam et al., 2019). Van Dam et al. (2019) validated the use of wind speed at 10 m above the water's surface (U_{10}) to estimate gas transfer velocities of CO_2 that were standardized to a Schmidt number of 600 (k_{600}) by comparing estimated values to k_{600} values derived directly from eddy covariance CO_2 flux measurements. Given the relative uniformity of wind speed over the Rhode River where median binned U_{10} windspeed (converted from U_7 measurements) was 2.2 m · s^{-1} regardless of time of day or season, and that maximum values rarely exceeded 10 m s^{-1} (Table 1, Fig. S1), we chose to use the most conservative estuarine-specific parameterization of k_{600} (Van Dam et al., 2019) (Eq. 2). The mean overall Rhode River k_{600} value for CO_2 (mean ± SD, 7.86 ± 2.05 cm · hr^{-1}) was of comparable magnitude to that of the New River Estuary, NC (9.37 ± 9.47 cm · hr^{-1}. However, wind speed varied far less on the Rhode River than the New River estuary and day/night explained more variability in wind speed than season. Because wind speed directly influenced the formulation of k_{600} (Eq. 2), the effect size of day/night is similarly greater than the seasonal effect on gas transfer velocity (Table 2). Nevertheless, effect sizes (ω^2) indicate that "season" explained at least 10 times more of the observed variance of *p*CO2water, *p*CO2air, air-water concentration gradient, CO2 flux, and gas-specific solubility than "day/night" or their interaction (Table 2). Given the minor freshwater input and microtidal nature of the Rhode River, we do not believe that lateral water velocity and bottom turbulence appreciably affect the gas transfer velocity of CO_2 here, although we did not investigate possible influences explicitly.

Importantly, in coastal marine and estuarine habitats, ΔC can shift as much as several thousand μatm per day due to diel cycling associated with CO_2 production and depletion (Figs. 2, S2). The uncertainty surrounding gas transfer velocity parameterization can represent a major source of error in CO_2 flux calculations (Frankignoulle et al., 1998; Upstill-Goddard, 2006; Wanninkhof & McGillis, 1999); however, small errors in k_{600} have far less effect on CO_2 flux calculations in estuaries which experience pCO_2 swings of several thousand μatm during a single day, compared with more stable conditions of the open ocean where interannual ranges of pCO_2 are typically far less (Van Dam et al., 2019).

3.6 CO_2 flux - Seasonality and Interannual Variation

CO_2 flux was determined according to Eq. 3 using hourly ΔC measurements, CO_2 solubility values (K_0) calculated according to temperature and salinity, and estuary-specific standardized gas transfer velocities (k_{600}) of Van Dam et al. (2019). CO_2 flux was plotted across the three years of observations at hourly and monthly intervals (Fig. 4a-b). As observed with pCO_2, CO_2 flux in the Rhode River was shown to be strongly seasonal. Given the similarity in windspeed across seasons (Fig. S1), the effect of differential mean ΔC and variation between warm- and cold-water seasons (Fig. 2, Table 1) almost certainly drives the observed seasonal differences in CO_2 flux (Fig. 4). Again, the specific solubility of CO_2 is greatest at low temperatures, yet this is contrary to the observed mean pCO_{2water} patterns, pointing toward a biological mechanism for pCO_2, ΔC, and ultimately, CO_2 flux. The effect size of season on CO_2 flux was two orders of magnitude greater than either day/night or the season day/night by interaction (Table 2).

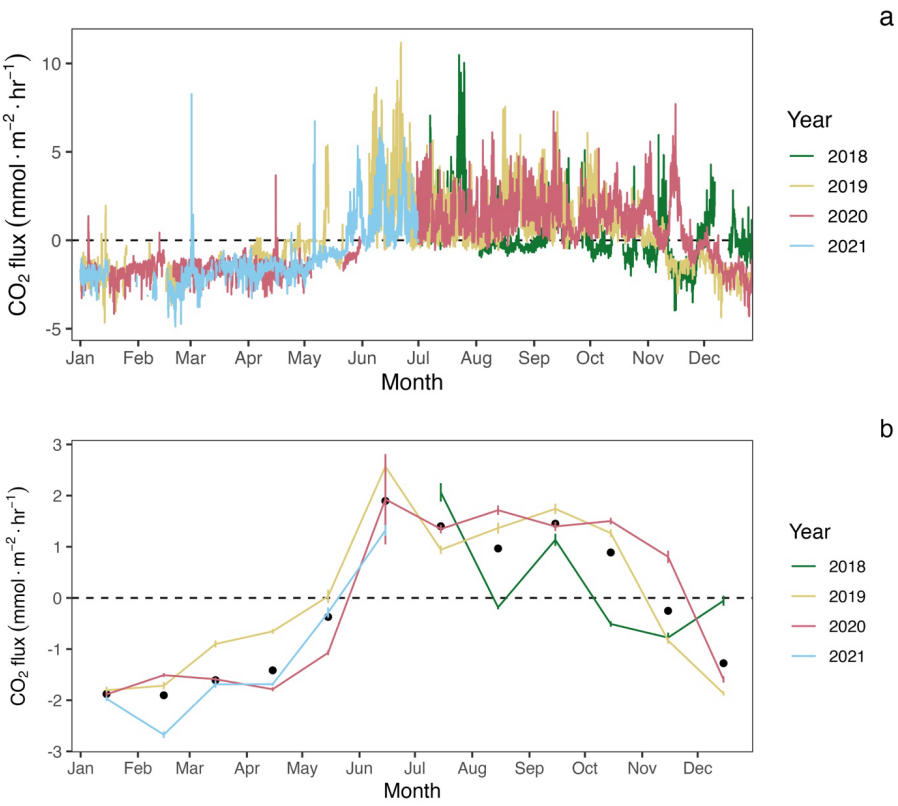

Fig. 4. CO_2 flux estimates by year: a. Hourly, b. Monthly average CO_2 flux estimates with 95% confidence limits. Black dots in panel b indicate mean monthly fluxes across years.

Among years, pCO_{2water} and CO_2 flux largely repeat themselves, with dissolved CO_2 becoming consistently sub-atmospheric and CO_2 flux going negative (gas exchange from atmosphere to water) between December and May and abruptly transitioning to much higher maximum, yet variable pCO_{2water} values with net positive CO_2 fluxes from June through November (Figs. 2 and 4). Monthly averaged CO_2 fluxes are consistent among years (Fig. 4b), with net positive CO_2 fluxes (heterotrophic conditions) between June and November and negative (autotrophic) fluxes dominating when water temperatures are cold, between December and May. Despite the overall

similarities in seasonal CO_2 flux, inter-annual patterns can vary considerably. When hourly CO_2 flux values were averaged for the year, the Rhode River in 2019 was shown to have a net positive flux but a net negative flux in 2020. When scaled for the year, 2019 outgassed CO_2 from the water to the atmosphere at a rate of 2215.08 mmol $\cdot$ m^{-2} $\cdot$ yr^{-1} (95% CI = 1816.88, 2613.29). The annual net flux rate in 2020 was negative (i.e. CO_2 moved from the atmosphere into the river) at a rate of -1361.31 mmol $\cdot$ m^{-2} $\cdot$ yr^{-1} (95% CI = -1723.60, -999.01).

At shorter time scales, such as comparing the same week of the year among years, we sometimes observed vast differences in the magnitude and direction of CO_2 flux (Fig. S3), signaling differences in seasonal conditions between years. Transient events can also result in deviations from otherwise typical CO_2 flux conditions. For example, the period from July 2018 to Jan 2019 deviated from other years as CO_2 flux was more erratic, with intermittent periods of negative and positive CO_2 flux extending later into the winter season than in other years. When water temperatures are compared among years, 2018 was shown to be more inconsistent, with more pronounced temperature shifts and reversals than in 2019 or 2020 (Fig. S1). Salinities remained relatively low for the latter half of 2018 into early 2019, reflecting wetter conditions (Fig. S1). There were also two rapid salinity declines (>4 ppt reductions) in July and October 2018, likely associated with strong precipitation events. These events were both followed by immediate spikes in chlorophyll-*a* concentration to levels exceeding 200 μg $\cdot$ L^{-1}, indicative of phytoplankton bloom conditions. From 2018 to 2021, chlorophyll-*a* levels of this magnitude and greater were generally confined to cold-water months (Dec–May; Fig. S1 Erratic water temperature and salinity are also reflected in more variable gas-specific solubility (K_0) for CO_2 in 2018 than later years (Fig. 3).

Gallegos et al. (1992) documented predictable phytoplankton blooms associated with freshets in the Rhode River, when nutrient-rich freshwater inundates the estuary, not from point and non-point sources within the local Rhode River watershed, but instead from the enormous watershed that feeds the Susquehanna River, the primary source of freshwater input into the Chesapeake above the Potomac as well as >50% of the entire Bay's freshwater (U.S. Geological Survey, 2023). Unlike river dominated estuaries, in the Rhode River estuary, volumetric influxes from the Chesapeake Bay end member far exceed freshwater input from the Muddy Creek and

541 secondary tributaries. In the Rhode River, phytoplankton blooms result in the temporary
542 depletion of pCO_{2water}, followed by a spike, as phytoplankton senesce and organic carbon is
543 decomposed/re-mineralized back into inorganic carbon. Episodic, short-lived occurrences like
544 these demonstrate how immediate small scale biological forcing, can be coupled with, and
545 catalyzed by, distant large-scale weather and hydrological events. These in turn can influence
546 pCO_2 flux variations within seasons and among years (Fig. 3 and S3; and Chen et al., 2020).
547
548 Overall, except for wind speed, the effect sizes for the other six measured or calculated variables
549 were shown to be greatest for season vs. day/night or the interaction of season x day/night, and in
550 all cases the season effect was greater by at least 1 order of magnitude (Table 2). Seasonality has
551 10 to 1000 times more explanatory power than other variables investigated as estimated by ω^2
552 (Table 2).
553
554 3.7 Shifting Net Ecosystem Production
555 To better understand how the net ecosystem production (NEP) of the Rhode River shifts
556 throughout the year, where positive NEP indicates the river is storing carbon (autotrophic state)
557 and negative NEP indicates it is releasing carbon to the atmosphere (heterotrophic state), we
558 calculated hourly CO_2 flux values, averaged them by day (i.e. 24 hr period) and plotted each in
559 relation to the $\Delta C = 0$ reference. Each day of the 3 yr study was categorized as either net
560 heterotrophic (CO_2 flux from water to atmosphere) or net autotrophic (CO_2 flux from atmosphere
561 to water). Each day was then further identified as either purely heterotrophic (all 24 hours were
562 heterotrophic), purely autotrophic, or mixed (some hours were heterotrophic and some were
563 autotrophic but resulting in a net autotrophic or net heterotrophic state for the day) (Fig. 5). From
564 July 2018 to July 2021, most 24 hr periods were categorized as pure autotrophic (444/920 =
565 48%), while 25% (229/990) were purely heterotrophic, and the remainder of mixed trophic status
566 (17% net heterotrophic and 10% net autotrophic; Fig. 5).
567

Deleted: ¶

Deleted: 3.7 Diel Cycling ¶
The notion that estuaries are predominantly heterotrophic systems that invariably outgas more CO_2 to the atmosphere than they absorb has been a long-held view (Abril et al., 2000; Borges et al., 2004; Cai, 2011; Cai et al., 2000; Chen, 2013; Frankignoulle et al., 1998, Gattuso et al., 1998). However, more recently investigators have realized that physical and hydrological characteristics, geographical location, size, and biological and biogeochemical activities may individually, or together, influence CO_2 flux in estuaries and therefore contributions to atmospheric chemistry (Brodeur et al. 2019; Caffrey, 2004; Chen et al., 2013, 2020; Herrmann et al., 2020). Furthermore, inadequate sampling can induce bias (e.g., upscaling from a small number of daytime samples taken during warm-water months can skew apparent patterns; Laruelle et al., 2017; Van Dam et al., 2019.) Using 1 minute sampling intervals, averaged to the hour, reveals patterns in the Rhode River that might otherwise be overlooked. We document the Rhode River as having strong seasonality in both pCO_2 content as well as the extent and direction of CO_2 flux (Figs. 2, S1, S2). Both measures are marked by daily oscillations, frequently reversing direction during a single 24 hr period in warm-water months (Figs. 2) but more stable and unidirectional during cold-water months (Figs. 2 and 5). ¶

Deleted: 8

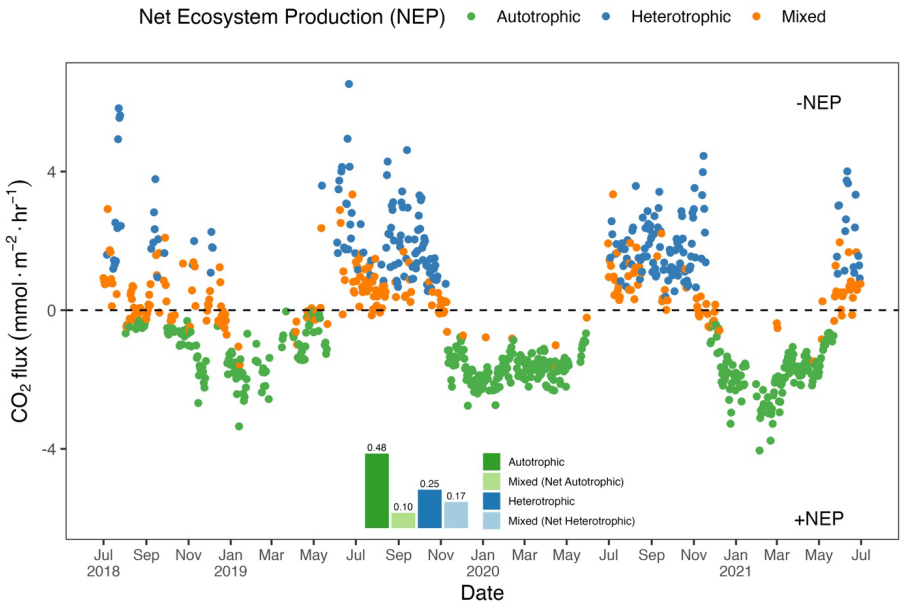

Fig. 5. Daily mean CO_2 flux estimates (CO_2 gradient is $CO_{2water} - CO_{2air}$). Green dots indicate days when all 24 hourly flux measurements were negative (autotrophic with +NEP); blue dots indicate days on which all 24 hourly flux measurements were positive (heterotrophic with -NEP). Orange dots indicate that hourly fluxes were both negative and positive, and the position of the orange dot below or above the zero line indicates whether the day was net autotrophic or net heterotrophic. Insert describes the proportion of days in each category indicating that during 58% (0.48 + 0.10) of days across three years of observation, the Rhode River was a CO_2 sink.

Altogether, the Rhode River was net autotrophic for (535 of 920 days = 58%) and net heterotrophic for 42% (385 days) across three years. When CO_2 flux is integrated over all three years, the Rhode River is shown to have near neutral NEP (Fig. 6). The effect size of season is two orders of magnitude greater than either that of day/night or season:day/night interaction (Table 2). Mean CO_2 flux values highlight the obvious correlation between season and NEP; error bars (± 1 SD) reveal the importance of diel cycling where the magnitude and directionality of day/night flux variability is approximately equal to the overall variability accrued across all three years (Fig. 6). Although CO_2 flux is less variable and more autotrophic during cold-water

613 months than warm-months in the Rhode River, the range of possible values that occur across
614 night and day, regardless of season, must be taken into consideration to minimize incidental
615 sampling bias (Figs. 2 and 6).
616
617 A multi-year investigation of CO_2 flux in the main stem of Chesapeake Bay by Chen et al.
618 (2020) combined several bay-wide cruises that were distributed across seasons to collect discrete
619 and underway pCO_2 data for CO_2 flux calculations. They concluded that the low salinity upper
620 bay, which receives large volumes of freshwater from the Susquehanna River, was net
621 heterotrophic; the mesohaline middle bay was net autotrophic, and the polyhaline lower bay was
622 near carbon neutral. Chen et al. (2020) characterized Chesapeake Bay, on the whole, as a weak
623 source of CO_2 to the atmosphere (net flux = 0.73 mol $\cdot$ m^{-2} $\cdot$ yr^{-1}) but suggested that during wet
624 years, it may function as weak sink of CO_2. Herrmann et al. (2020) also concluded that the
625 Chesapeake Bay was a weak source of CO_2 to the atmosphere based on calculated pCO_2 values
626 from long term pH and alkalinity measurements (net flux = 1.2 mol $\cdot$ m^{-2} $\cdot$ yr^{-1}mol). Brodeur and
627 colleagues (2019) examined dissolved inorganic carbon (DIC) and total alkalinity along the
628 mainstem of the Chesapeake Bay across the year in 2016 and concluded that DIC increases from
629 north to south and from surface waters to depth, but that seasonal riverine input and biological
630 cycling were significantly important, concluding that the Bay as a whole was a sink for CO_2.
631
632 When our annual mean pCO_2 values were compared with the Chen et al. (2020) survey, the
633 Rhode River was shown to be higher on average and more variable than the mesohaline main
634 stem of the Bay (591 ± 652 vs. 416 ± 167 μatm), including a substantially greater measured
635 range (min = 15, max = 5182 μatm vs. 103 and 1033 μatm). These results suggest that water in
636 the shallow and well mixed Rhode River, and DIC in particular, undergo more acute biological
637 transformation than in the mesohaline main stem of Chesapeake Bay. Chen et al. (2020) point to
638 a variety of factors that affect pCO_2 and CO_2 flux in the main stem bay, including temperature,
639 depth, stratification, and freshwater input volume, some of which may attenuate biological
640 forcing. Interannual variability was demonstrated in both the Rhode River (some years were net
641 autotrophic and others heterotrophic, Figs. 4 and 5) and in the mesohaline main stem of the Bay;
642 however, we attribute interannual variability in pCO_2 and CO_2 flux primarily to variation in
643 water temperature that in turn drives biological activity. We conclude that seasonal variations the

644 Rhode River (and likely similar rivers in the mesohaline portion of the Chesapeake) are
645 significant and predictable, closely associated with water temperature, and that temperature
646 mediates NEP biologically rather than by changes to the solubility of CO_2.

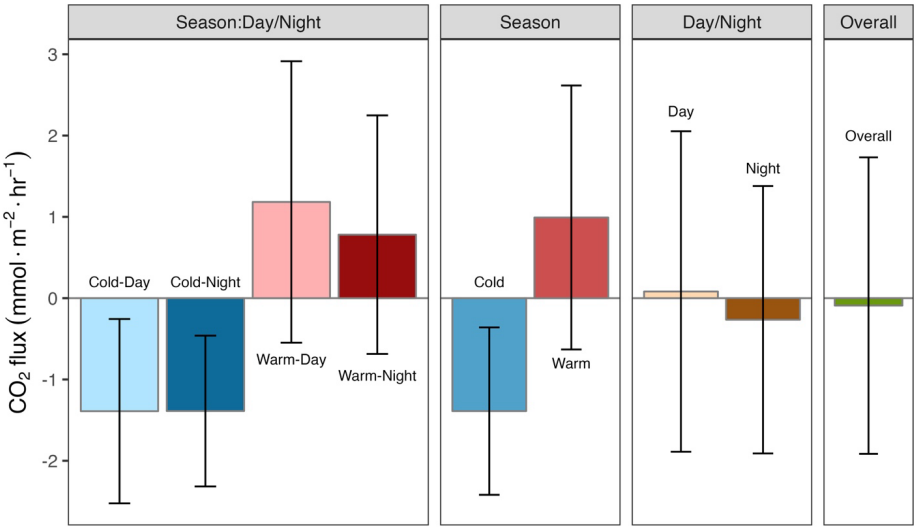

647
648

649 **Fig. 6.** Mean CO_2 flux ± 1 SD (mmol · m^{-2} · hr^{-1}) plotted by day/night cycling, cold-water/warm-
650 water season, season by day/night interaction, and overall CO_2 flux across three years of
651 observation.
652

653 In the Rhode River, we find that CO_2 flux reverses itself daily for part of the year (June–
654 November) yielding some days that are characterized as a net sink (net autotrophic) and others
655 that are a net source (net heterotrophic). From December to May, diel cycling is minimal and the
656 river is almost exclusively a net sink, autotrophic both day and night. Finally, although CO_2 flux
657 is pronounced but variable across seasons, the net CO_2 flux of the Rhode River on an annual
658 basis is near neutral.
659
660
661
662

3.8 Lateral transport

Deleted: 9

Tidal cycling has been shown to liberate and laterally transport DOC from brackish marshes to adjacent estuaries (Cai, 2011; Herrmann, 2015) and therefore is of great importance to carbon cycling and budgets of wetlands and estuaries (Najjar et al., 2020). DOC outwelling from the Kirkpatrick Marsh (hereafter KPM), a 0.21 km^2 tidal marsh located approximately 1 km up estuary from our primary study site at the SERC Dock (Fig. 1), into the Rhode River has been measured and modeled extensively in recent years (Clark et al., 2020; Menendez et al., 2022; Tzortziou et al., 2011; Tzortziou et al., 2008). These studies indicate that the KPM is responsible for a large portion of overall DOC input to the Rhode River, as well as significant export from the river to the mainstem of Chesapeake Bay. Model generation and validation by Clark et al. (2020) indicate that up to 13.1% of the total DOC input to the Rhode River originates in the KPM. Another important source (53% of total) is DOC derived from phytoplankton and is therefore labile and readily biodegraded and remineralized into DIC. Furthermore, large quantities of other, semi-labile forms of DOC are exported from the KPM, which are themselves subject to photochemical and biodegradation and remineralization (Clark et al., 2020). Importantly, each of these DOC streams provides a potential source of DIC, including pCO_2, to the Rhode River.

Dissolved inorganic carbon generated in brackish tidal wetlands is also outwelled directly into estuaries (e.g., Cai et al., 2000; Chu et al., 2018; Song et al., 2023). Recent work by Song et al. (2023) demonstrates that pCO_2 in a salt marsh tidal creek in Waquoit Bay, MA was regulated by both tide height (inversely) and the day/night cycle, with nighttime low tides resulting in the highest pCO_2 values, signaling a strong local effect from respiration and photosynthesis in combination with tidal outwelling.

In the Rhode River watershed pCO_2 was measured continuously in the single tidal creek that drains the KPM using the same methods as at our primary study location. We observed that the KPM tidal creek pCO_2 follows the tidal cycle exclusively, yet outside the mouth of the tidal creek, in the estuary proper, day/night cycling overwhelms this marsh tidal signal. Simultaneous pCO_2 measurements from the SERC dock follow a strict day/night cycle (Fig. S4). However, while peak levels of dissolved CO_2 in the Kirkpatrick Marsh creek occur at low tide and can

reach values nearly 20 times greater than highs at the SERC dock (Fig. S4) there is no obvious evidence of this tidal DIC input at the dock site. Remineralization of DOC exported from the KPM, as well as DOC originating in other locations within the watershed are important sources of DIC in the river, but given the relative volumes of these sources to that of the much larger estuary, as well as the physical distance (~1 km) from SERC dock, these input signals should be expected to be lagged and damped inside the estuary and not tightly coupled with tidal cycles. Instead, pCO_2 exported from the KPM is expected to undergo significant dilution effects, be partially off-gassed to the atmosphere, and be metabolized via photosynthesis, reducing its influence on downstream sites. These findings suggest that despite periodic extreme pCO_2 in KPM tidal creek (>30,000 ppmv), the overall mass of CO_2 export is not sufficient to have measurable effects on the deeper, well-mixed portions of the Rhode River.

Thus, although land – sea interfaces and outwelling of DOC and DIC are important in estuaries and coastal ecosystems, the relative sizes of wetlands and adjacent water bodies and the overall volume of water moving between the two are also important factors. In eutrophic estuaries like the Rhode River, biological forcing can rapidly assimilate DIC and degrade and mineralize labile forms of DOC, as evidenced by extensive diel cycling in these systems (e.g., Brodeur et al. 2019; Song et al. 2023, and the present study.) The much larger and complex Chesapeake Bay generally follows seasonal changes in pCO_2 and CO_2 flux, but these appear to be most predictable in the upper oligohaline portion and the polyhaline region of the bay near the mouth, where freshwater and oceanic end-member effects are most pronounced (Brodeur et al. 2019; Chen et al., 2020). The central mesohaline part of Chesapeake Bay comprises numerous discrete and unique watersheds and subestuaries/rivers, each of which exchanges water with the bay. Elucidating spatial and temporal patterns of pCO_2 and CO_2 flux are vital for understanding each one's role as an atmospheric source or sink, but also could provide better insight into how each may be influenced by global increases in atmospheric CO_2 (i.e., acidification and its influences on estuarine metabolism, and the local biota, fisheries, and habitats each support.) Collectively, these and other subestuaries will have cumulative effects on the overall water quality of Chesapeake Bay, including cycling of DOC and DIC, which in turn affect pCO_2 and CO_2 flux.

4. Conclusion

The notion that estuaries are predominantly heterotrophic systems that invariably outgas more CO_2 to the atmosphere than they absorb has been a long-held view (Abril et al., 2000; Borges et al., 2004; Cai, 2011; Cai et al., 2000; Chen, 2013; Frankignoulle et al., 1998, Gattuso et al., 1998). However, more recently investigators have realized that physical and hydrological characteristics, geographical location, size, and biological and biogeochemical activities may individually, or together, influence CO_2 flux in estuaries and therefore contributions to atmospheric chemistry (Brodeur et al. 2019; Caffrey, 2004; Chen et al., 2013, 2020; Herrmann et al., 2020). As indicated in this study and others, the role that biological processes play in estuaries to either fix CO_2 (autotrophy) or liberate CO_2 (heterotrophy) are extensive, complex, and can be quite variable over space and time (Brodeur et al. 2019; Chen et al., 2020; Herrmann et al., 2020; Rosentreter et al., 2021). High frequency automated measurements revealed strong seasonal contrasts in dissolved CO_2 content and CO_2 flux between water and atmosphere of the Rhode River, a shallow mesohaline reach of the Chesapeake Bay. Importantly, only through high frequency, multi-year measurements could diel and seasonal cycling be fully discerned. Indeed, inadequate sampling can induce bias (e.g., upscaling from a small number of daytime samples taken during warm-water months can skew apparent patterns; Laruelle et al., 2017; Van Dam et al., 2019.). The timing and frequency of measurements are critical and have potential for strong and misleading biases if sampling is insufficient. In contrast, cold-water months coincide with long periods (weeks to months) of continuous sub-atmospheric sink conditions for CO_2. Using these measurements, we estimated the direction and magnitude of CO_2 flux in hourly, daily, and annual terms. In the Rhode River CO_2 flux reverses itself daily for part of the year (June through November) yielding some days that are characterized as net sink (net autotrophic and NEP > 0) and others that are net source (net heterotrophic and NEP < 0). From December to May diel cycling is minimal, and the river is almost exclusively a CO_2 sink with +NEP both day and night. Although CO_2 flux is pronounced but variable across seasons, the net CO_2 flux of the Rhode River on an annual basis is near carbon neutral, although some years are net heterotrophic and others net autotrophic.

High frequency sampling of pCO_2, although typically confined spatially, is one approach to understanding fundamental aspects of estuarine metabolic states and CO_2 flux that may

otherwise go undetected (Song et al., 2023). To address the spatial complexity of estuarine, nearshore, and inland waters, more observation locations are required. As with any environmental or ecological question, careful sampling design is critical to balance efficiency and statistical power.

As the largest and arguably most complex estuary in the United States, the Chesapeake Bay is the subject of extensive ecosystem management efforts and ranks among the most studied and monitored estuaries in the world (Boesch and Goldman 2009). Yet, information on CO_2 and GHG fluxes continue to be limited (Brodeur 2019; Chen et al., 2020; Herrmann et al., 2020). Given the extensive coordinated monitoring programs that either make real-time water quality measurements and/or maintain routine water sampling schedules (e.g., Maryland DNR "Eyes on the Bay" program) in this region, existing water quality observation assets and sampling programs could be leveraged to more fully characterize and quantify CO_2 and other GHG dynamics and flux in the Bay and elsewhere (see Saba et al. 2019). For example, coordinated deployment of additional automated sampling devices (e.g., robust air-water equilibrators and traditional atmospheric gas sensors) in key locations would enable estimates of CO_2 flux, and if combined with pH, DIC, or total alkalinity measurements, carbonate chemistry calculations as well. Importantly, such installations need not be permanent. Instead, a small group of instruments could be systematically deployed across an existing observation network, co-located with other water quality instruments using a stratified sampling approach to capture spatial variability. For example, a set of shifting two to four week deployments during summer and winter months could yield sufficient data to advance our understanding of Chesapeake Bay-wide CO_2 flux significantly in a single year. Such information would complement underway transects that are vital, but which tend to underestimate temporal variability in any given location. In the case of dissolved GHGs, liquid-air equilibration techniques are being used to measure multiple GHGs (Call et al. 2015; Hartmann 2018; Gülzow et al. 2011; Miller et al. 2019; Xiao et al. 2020).

Understanding the GHG dynamics in estuaries is a vital component to generating accurate global budgets (Maher & Eyre, 2012) as well as informing where emerging carbon capture technologies, including nature-based solutions, might be best located (Bradshaw & Dance, 2005;

Sun et al., 2021). In the case of estuaries, there have been extensive global losses of seagrasses due to habitat degradation, pollution, and disease (Waycott et al. 2009). In addition to many other ecosystem service benefits, restoration of seagrass and submerged aquatic vegetation has the potential to restore and enhance natural carbon sequestration (i.e. blue carbon; Kennedy et al. 2022; Macreadie et al. 2022; Unsworth et al. 2022). In Virginia, U.S.A., Oreska et al. (2020) demonstrated how the functional benefits of a restored seagrass meadow habitat can be quantified ecologically in terms of their ability to sequester carbon and affect GHG fluxes between the estuary and atmosphere. Uniquely, these investigators then monetized the costs and benefits of habitat restoration and function as CO_2 offset credits, as part of a GHG budget, and demonstrated how such approaches can be used to incentivize habitat restoration (Oreska et al. (2020).

Increasing the completeness and utility of global GHG budgets, as they relate to human activities and ecosystem functions, are necessary steps toward combating global climate change. Measurement of GHGs at high spatial and temporal resolution using economical, automated measurement solutions can increase our understanding of GHG dynamics at small ecologically significant scales, as well as at the larger ecosystem level of an estuary.

Data Availability

Hourly means of pCO_2 and associated environmental data used in the analyses are available at the Smithsonian Figshare repository https://doi.org/10.25573/serc.22491655 via under Creative Commons license CC BY-NC 4.0.

Author Contributions

AWM contributed to project Conceptualization, Funding acquisition, Investigation, Methodology, Project Administration, Resources, Supervision and Writing – Original Draft. JRM contributed to Data Curation, Formal Analysis, Software and Visualization. ACR contributed to Data Curation, Investigation, Methodology and Project Administration. MSM contributed to Conceptualization, Supervision and Visualization. KJK contributed to Conceptualization, Data Curation, Software, Validation. All authors contributed to Writing – review and editing.

Competing Interests

The corresponding author has declared that none of the authors has any competing interests.

Deleted: ¶
¶
¶

Acknowledgments

We thank Patrick Neale and Stephanie Wilson for their early review and critical feedback on this manuscript, as well as J. Patrick Megonigal for discussions on methodology and two anonymous reviewers who contributed beneficial suggestions. Funding for this research was provided by the Smithsonian Institution.

References

Abril, G. and Borges, A. V.: Carbon Dioxide and Methane Emissions from Estuaries, in: Greenhouse Gas Emissions — Fluxes and Processes: Hydroelectric Reservoirs and Natural Environments, edited by: Tremblay, A., Varfalvy, L., Roehm, C., and Garneau, M., Springer, Berlin, Heidelberg, 187–207, https://doi.org/10.1007/978-3-540-26643-3_8, 2005.

Abril, G., Etcheber, H., Borges, A. V., and Frankignoulle, M.: Excess atmospheric carbon dioxide transported by rivers into the Scheldt estuary, Comptes Rendus de l'Académie des Sciences - Series IIA - Earth and Planetary Science, 330, 761–768, https://doi.org/10.1016/S1251-8050(00)00231-7, 2000.

Bauer, J. E., Cai, W.-J., Raymond, P. A., Bianchi, T. S., Hopkinson, C. S., and Regnier, P. A. G.: The changing carbon cycle of the coastal ocean, Nature, 504, 61–70, https://doi.org/10.1038/nature12857, 2013.

Benson, S., Rich, R., Tashjian, A., Lonneman, M., and Neale, P.: MarineGEO Upper Chesapeake Bay Observatory CPOP Data, https://doi.org/10.25573/SERC.C.6100368.V10, 2023.

Boesch, D.F. and Goldman, E.B.: Chesapeake Bay, USA, in: Ecosystem-Based Management for the Oceans, edited by: McLeod, K. McLeod and Leslie H. Island Press, Washington, D.C., 268–

293, 2009.

Borges, A. V.: Do we have enough pieces of the jigsaw to integrate CO2 fluxes in the coastal ocean?, Estuaries, 28, 3–27, https://doi.org/10.1007/BF02732750, 2005.

Borges, A. V., Delille, B., Schiettecatte, L.-S., Gazeau, F., Abril, G., and Frankignoulle, M.: Gas transfer velocities of CO2 in three European estuaries (Randers Fjord, Scheldt, and Thames), Limnology and Oceanography, 49, 1630–1641, 2004.

Bradshaw, J. and Dance, T.: Mapping geological storage prospectivity of CO2 for the world's sedimentary basins and regional source to sink matching, in: Greenhouse Gas Control Technologies 7, vol. I, Elsevier, 583–591, https://doi.org/10.1016/B978-008044704-9/50059-8, 2005.

Breitburg, D. L., Hines, A. H., Jordan, T. E., McCormick, M. K., Weller, D. E., and Whigham, D. F.: Landscape patterns, nutrient discharges, and biota of the Rhode River estuary and its watershed: Contribution of the Smithsonian Environmental Research Center to the Pilot Integrated Ecosystem Assessment, 2008.

Brodeur, J. R., Chen, B., Su, J., Xu, Y.-Y., Hussain, N., Scaboo, K. M., Zhang, Y., Testa, J. M., and Cai, W.-J.: Chesapeake Bay Inorganic Carbon: Spatial Distribution and Seasonal Variability, Frontiers in Marine Science, 6, https://doi.org/10.3389/fmars.2019.00099, 2019.

Broecker, W. S., Takahashi, T., Simpson, H. J., and Peng, T.-H.: Fate of Fossil Fuel Carbon Dioxide and the Global Carbon Budget, Science, 206, 409–418, 1979.

Caffrey, J. M.: Factors controlling net ecosystem metabolism in US estuaries, Estuaries, 27, 90–101, 2004.

Cai, W.-J.: Estuarine and Coastal Ocean Carbon Paradox: CO2 Sinks or Sites of Terrestrial Carbon Incineration?, Annual Review of Marine Science, 3, 123–145, https://doi.org/10.1146/annurev-marine-120709-142723, 2011.

Cai, W.-J. and Wang, Y.: The chemistry, fluxes, and sources of carbon dioxide in the estuarine waters of the Satilla and Altamaha Rivers, Georgia, Limnology and Oceanography, 43, 657–668, https://doi.org/10.4319/lo.1998.43.4.0657, 1998.

877 Cai, W.-J., Wiebe, W. J., Wang, Y., and Sheldon, J. E.: Intertidal marsh as a source of dissolved
878 inorganic carbon and a sink of nitrate in the Satilla River-estuarine complex in the southeastern
879 U.S., Limnology and Oceanography, 45, 1743–1752, https://doi.org/10.4319/lo.2000.45.8.1743,
880 2000.

881 Call, M., Maher, D. T., Santos, I. R., Ruiz-Halpern, S., Mangion, P., Sanders, C. J., Erler, D. V.,
882 Oakes, J. M., Rosentreter, J., Murray, R., and Eyre, B. D.: Spatial and temporal variability of
883 carbon dioxide and methane fluxes over semi-diurnal and spring–neap–spring timescales in a
884 mangrove creek, Geochimica et Cosmochimica Acta, 150, 211–225,
885 https://doi.org/10.1016/j.gca.2014.11.023, 2015.

886 Chen, B., Cai, W.-J., Brodeur, J. R., Hussain, N., Testa, J. M., Ni, W., and Li, Q.: Seasonal and
887 spatial variability in surface pCO2 and air–water CO2 flux in the Chesapeake Bay, Limnology
888 and Oceanography, 65, 3046–3065, https://doi.org/10.1002/lno.11573, 2020.

889 Chen, C.-T. A., Huang, T.-H., Chen, Y.-C., Bai, Y., He, X., and Kang, Y.: Air–sea exchanges of
890 CO2 in the world's coastal seas, Biogeosciences, 10, 6509–6544, https://doi.org/10.5194/bg-10-
891 6509-2013, 2013.

892 Chu, S. N., Wang, Z. A., Gonneea, M. E., Kroeger, K. D., and Ganju, N. K.: Deciphering the
893 dynamics of inorganic carbon export from intertidal salt marshes using high-frequency
894 measurements, Marine Chemistry, 206, 7–18, https://doi.org/10.1016/j.marchem.2018.08.005,
895 2018.

896 Clark, J. B., Long, W., Tzortziou, M., Neale, P. J., and Hood, R. R.: Wind-Driven Dissolved
897 Organic Matter Dynamics in a Chesapeake Bay Tidal Marsh-Estuary System, Estuaries and
898 Coasts, 41, 708–723, https://doi.org/10.1007/s12237-017-0295-1, 2018.

899 Clark, J. B., Long, W., and Hood, R. R.: A Comprehensive Estuarine Dissolved Organic Carbon
900 Budget Using an Enhanced Biogeochemical Model, Journal of Geophysical Research:
901 Biogeosciences, 125, e2019JG005442, https://doi.org/10.1029/2019JG005442, 2020.

902 Correll, D. L., Jordan, T. E., and Weller, D. E.: Nutrient flux in a landscape: Effects of coastal
903 land use and terrestrial community mosaic on nutrient transport to coastal waters, Estuaries, 15,
904 431–442, https://doi.org/10.2307/1352388, 1992.

905 Dai, M., Su, J., Zhao, Y., Hofmann, E. E., Cao, Z., Cai, W.-J., Gan, J., Lacroix, F., Laruelle, G.
906 G., Meng, F., Müller, J. D., Regnier, P. A. G., Wang, G., and Wang, Z.: Carbon Fluxes in the
907 Coastal Ocean: Synthesis, Boundary Processes, and Future Trends, Annual Review of Earth and
908 Planetary Sciences, 50, 593–626, https://doi.org/10.1146/annurev-earth-032320-090746, 2022.

909 Frankignoulle, M., Abril, G., Borges, A., Bourge, I., Canon, C., Delille, B., Libert, E., and
910 Théate, J.-M.: Carbon Dioxide Emission from European Estuaries, Science, 282, 434–436,
911 https://doi.org/10.1126/science.282.5388.434, 1998.

912 Freeman, L. A., Corbett, D. R., Fitzgerald, A. M., Lemley, D. A., Quigg, A., and Steppe, C. N.:
913 Impacts of urbanization and development on estuarine ecosystems and water quality, Estuaries
914 and Coasts, 42, 1821–1838, https://doi.org/10.1007/s12237-019-00597-z, 2019.

915 Freshwater Flow into Chesapeake Bay | U.S. Geological Survey:
916 https://www.usgs.gov/centers/chesapeake-bay-activities/science/freshwater-flow-chesapeake-
917 bay, last access: 21 September 2023.

918 Gallegos, C. L., Jordan, T. E., and Correll, D. L.: Event-scale response of phytoplankton to
919 watershed inputs in a subestuary: Timing, magnitude, and location of blooms, Limnology and
920 Oceanography, 37, 813–828, https://doi.org/10.4319/lo.1992.37.4.0813, 1992.

921 Gallegos, C. L., Jordan, T. E., and Hedrick, S. S.: Long-term Dynamics of Phytoplankton in the
922 Rhode River, Maryland (USA), Estuaries and Coasts, 33, 471–484,
923 https://doi.org/10.1007/s12237-009-9172-x, 2010.

924 Gattuso, J.-P., Frankignoulle, M., and Wollast, R.: Carbon and Carbonate Metabolism in Coastal
925 Aquatic Ecosystems, Annual Review of Ecology and Systematics, 29, 405–434,
926 https://doi.org/10.1146/annurev.ecolsys.29.1.405, 1998.

927 Gülzow, W., Rehder, G., Schneider, B., Deimling, J. S. v., and Sadkowiak, B.: A new method for
928 continuous measurement of methane and carbon dioxide in surface waters using off-axis
929 integrated cavity output spectroscopy (ICOS): An example from the Baltic Sea, Limnology and
930 Oceanography: Methods, 9, 176–184, https://doi.org/10.4319/lom.2011.9.176, 2011.

931 Hartmann, J. F., Gentz, T., Schiller, A., Greule, M., Grossart, H.-P., Ionescu, D., Keppler, F.,
932 Martinez-Cruz, K., Sepulveda-Jauregui, A., and Isenbeck-Schröter, M.: A fast and sensitive

933 method for the continuous in situ determination of dissolved methane and its δ13C-isotope ratio
934 in surface waters, Limnology and Oceanography: Methods, 16, 273–285,
935 https://doi.org/10.1002/lom3.10244, 2018.

936 Herrmann, M., Najjar, R. G., Kemp, W. M., Alexander, R. B., Boyer, E. W., Cai, W.-J., Griffith,
937 P. C., Kroeger, K. D., McCallister, S. L., and Smith, R. A.: Net ecosystem production and
938 organic carbon balance of U.S. East Coast estuaries: A synthesis approach, Global
939 Biogeochemical Cycles, 29, 96–111, https://doi.org/10.1002/2013GB004736, 2015.

940 Herrmann, M., Najjar, R. G., Da, F., Friedman, J. R., Friedrichs, M. A. M., Goldberger, S.,
941 Menendez, A., Shadwick, E. H., Stets, E. G., and St-Laurent, P.: Challenges in Quantifying Air-
942 Water Carbon Dioxide Flux Using Estuarine Water Quality Data: Case Study for Chesapeake
943 Bay, Journal of Geophysical Research: Oceans, 125, e2019JC015610,
944 https://doi.org/10.1029/2019JC015610, 2020.

945 Ho, D. T., Coffineau, N., Hickman, B., Chow, N., Koffman, T., and Schlosser, P.: Influence of
946 current velocity and wind speed on air-water gas exchange in a mangrove estuary, Geophysical
947 Research Letters, 43, 3813–3821, https://doi.org/10.1002/2016GL068727, 2016.

948 Jiang, L.-Q., Cai, W.-J., and Wang, Y.: A comparative study of carbon dioxide degassing in
949 river-and marine-dominated estuaries, Limnology and Oceanography, 53, 2603–2615, 2008.

950 Joesoef, A., Huang, W.-J., Gao, Y., and Cai, W.-J.: Air–water fluxes and sources of carbon
951 dioxide in the Delaware Estuary: spatial and seasonal variability, Biogeosciences, 12, 6085–
952 6101, https://doi.org/10.5194/bg-12-6085-2015, 2015.

953 Jordan, T. E. and Correll, D. L.: Continuous automated sampling of tidal exchanges of nutrients
954 by brackish marshes, Estuarine, Coastal and Shelf Science, 32, 527–545,
955 https://doi.org/10.1016/0272-7714(91)90073-K, 1991.

956 Jordan, T. E., Correll, D. L., Peterjohn, W. T., and Weller, D. E.: Nutrient flux in a landscape:
957 The Rhode River watershed and receiving waters, in: Watershed Research Perspectives, edited
958 by: Correll, D. L., Smithsonian Institution Press, Washington, DC, 1986.

Jordan, T. E., Correll, D. L., Miklas, J., and Weller, D. E.: Nutrients and chlorophyll at the interface of a watershed and an estuary, Limnol. Oceanogr., 36, 251–267, https://doi.org/10.4319/lo.1991.36.2.0251, 1991.

Kennedy, H., Pagès, J. F., Lagomasino, D., Arias-Ortiz, A., Colarusso, P., Fourqurean, J. W., Githaiga, M. N., Howard, J. L., Krause-Jensen, D., Kuwae, T., Lavery, P. S., Macreadie, P. I., Marbà, N., Masqué, P., Mazarrasa, I., Miyajima, T., Serrano, O., and Duarte, C. M.: Species Traits and Geomorphic Setting as Drivers of Global Soil Carbon Stocks in Seagrass Meadows, Global Biogeochemical Cycles, 36, e2022GB007481, https://doi.org/10.1029/2022GB007481, 2022.

Klaus, M. and Vachon, D.: Challenges of predicting gas transfer velocity from wind measurements over global lakes, Aquat Sci, 82, 53, https://doi.org/10.1007/s00027-020-00729-9, 2020.

Lachin, J. M.: Fallacies of last observation carried forward analyses, Clinical Trials, 13, 161–168, https://doi.org/10.1177/1740774515602688, 2016.

Laruelle, G. G., Goossens, N., Arndt, S., Cai, W.-J., and Regnier, P.: Air–water CO_2 evasion from US East Coast estuaries, Biogeosciences, 14, 2441–2468, https://doi.org/10.5194/bg-14-2441-2017, 2017.

Macreadie, P. I., Robertson, A. I., Spinks, B., Adams, M. P., Atchison, J. M., Bell-James, J., Bryan, B. A., Chu, L., Filbee-Dexter, K., Drake, L., Duarte, C. M., Friess, D. A., Gonzalez, F., Grafton, R. Q., Helmstedt, K. J., Kaebernick, M., Kelleway, J., Kendrick, G. A., Kennedy, H., Lovelock, C. E., Megonigal, J. P., Maher, D. T., Pidgeon, E., Rogers, A. A., Sturgiss, R., Trevathan-Tackett, S. M., Wartman, M., Wilson, K. A., and Rogers, K.: Operationalizing marketable blue carbon, One Earth, 5, 485–492, https://doi.org/10.1016/j.oneear.2022.04.005, 2022.

Maher, D. T. and Eyre, B. D.: Carbon budgets for three autotrophic Australian estuaries: Implications for global estimates of the coastal air-water CO2 flux, Global Biogeochemical Cycles, 26, https://doi.org/10.1029/2011GB004075, 2012.

Martin, C. R., Zeng, N., Karion, A., Dickerson, R. R., Ren, X., Turpie, B. N., and Weber, K. J.: Evaluation and environmental correction of ambient CO_2 measurements from a low-cost NDIR sensor, Atmospheric Measurement Techniques, 10, 2383–2395, https://doi.org/10.5194/amt-10-2383-2017, 2017.

Menendez, A., Tzortziou, M., Neale, P., Megonigal, P., Powers, L., Schmitt-Kopplin, P., and Gonsior, M.: Strong Dynamics in Tidal Marsh DOC Export in Response to Natural Cycles and Episodic Events From Continuous Monitoring, Journal of Geophysical Research: Biogeosciences, 127, e2022JG006863, https://doi.org/10.1029/2022JG006863, 2022.

Miller, A. W., Reynolds, A. C., and Minton, M. S.: A spherical falling film gas-liquid equilibrator for rapid and continuous measurements of CO2 and other trace gases, PLOS ONE, 14, e0222303, https://doi.org/10.1371/journal.pone.0222303, 2019.

Najjar, R. G., Herrmann, M., Cintrón Del Valle, S. M., Friedman, J. R., Friedrichs, M. A. M., Harris, L. A., Shadwick, E. H., Stets, E. G., and Woodland, R. J.: Alkalinity in Tidal Tributaries of the Chesapeake Bay, Journal of Geophysical Research: Oceans, 125, e2019JC015597, https://doi.org/10.1029/2019JC015597, 2020.

Oreska, M. P. J., McGlathery, K. J., Aoki, L. R., Berger, A. C., Berg, P., and Mullins, L.: The greenhouse gas offset potential from seagrass restoration, Sci Rep, 10, 7325, https://doi.org/10.1038/s41598-020-64094-1, 2020.

Raymond, P. A. and Cole, J. J.: Gas Exchange in Rivers and Estuaries: Choosing a Gas Transfer Velocity, Estuaries, 24, 312–317, https://doi.org/10.2307/1352954, 2001.

Raymond, P. A., Hartmann, J., Lauerwald, R., Sobek, S., McDonald, C., Hoover, M., Butman, D., Striegl, R., Mayorga, E., Humborg, C., Kortelainen, P., Dürr, H., Meybeck, M., Ciais, P., and Guth, P.: Global carbon dioxide emissions from inland waters, Nature, 503, 355–359, https://doi.org/10.1038/nature12760, 2013.

Rose, K. C., Neale, P. J., Tzortziou, M., Gallegos, C. L., and Jordan, T. E.: Patterns of spectral, spatial, and long-term variability in light attenuation in an optically complex sub-estuary, Limnology and Oceanography, 64, S257–S272, https://doi.org/10.1002/lno.11005, 2019.

1013 Rosentreter, J. A., Wells, N. S., Ulseth, A. J., and Eyre, B. D.: Divergent Gas Transfer Velocities
1014 of CO2, CH4, and N2O Over Spatial and Temporal Gradients in a Subtropical Estuary, Journal
1015 of Geophysical Research: Biogeosciences, 126, e2021JG006270,
1016 https://doi.org/10.1029/2021JG006270, 2021.

1017 Saba, G. K., Goldsmith, K. A., Cooley, S. R., Grosse, D., Meseck, S. L., Miller, A. W., Phelan,
1018 B., Poach, M., Rheault, R., St.Laurent, K., Testa, J. M., Weis, J. S., and Zimmerman, R.:
1019 Recommended priorities for research on ecological impacts of ocean and coastal acidification in
1020 the U.S. Mid-Atlantic, Estuarine, Coastal and Shelf Science, 225, 106188,
1021 https://doi.org/10.1016/j.ecss.2019.04.022, 2019.

1022 Saucier, W. J.: Principles of Meteorological Analysis, Dover Publications, 468 pp., 2003.

1023 Song, S., Wang, Z. A., Kroeger, K. D., Eagle, M., Chu, S. N., and Ge, J.: High-frequency
1024 variability of carbon dioxide fluxes in tidal water over a temperate salt marsh, Limnology and
1025 Oceanography, 68, 2108–2125, https://doi.org/10.1002/lno.12409, 2023.

1026 Spada, S., Quartagno, M., Tamburini, M., and Robinson, D.: orcutt: Estimate Procedure in Case
1027 of First Order Autocorrelation, 2018.

1028 Sun, X., Alcalde, J., Bakhtbidar, M., Elío, J., Vilarrasa, V., Canal, J., Ballesteros, J., Heinemann,
1029 N., Haszeldine, S., Cavanagh, A., Vega-Maza, D., Rubiera, F., Martínez-Orio, R., Johnson, G.,
1030 Carbonell, R., Marzan, I., Travé, A., and Gomez-Rivas, E.: Hubs and clusters approach to unlock
1031 the development of carbon capture and storage – Case study in Spain, Applied Energy, 300,
1032 117418, https://doi.org/10.1016/j.apenergy.2021.117418, 2021.

1033 Susquehanna River at Conowingo, MD | U.S. Geological Survey:
1034 https://waterdata.usgs.gov/monitoring-location/01578310/, last access: 28 September 2023.

1035 Takahashi, T., Sutherland, S. C., Sweeney, C., Poisson, A., Metzl, N., Tilbrook, B., Bates, N.,
1036 Wanninkhof, R., Feely, R. A., Sabine, C., Olafsson, J., and Nojiri, Y.: Global sea–air CO2 flux
1037 based on climatological surface ocean *p*CO2, and seasonal biological and temperature effects,
1038 Deep Sea Research Part II: Topical Studies in Oceanography, 49, 1601–1622,
1039 https://doi.org/10.1016/S0967-0645(02)00003-6, 2002.

1040 Thoning, K. W., Crotwell, A. M., and Mund, J. W.: NOAA Global Monitoring Laboratory
1041 Carbon Cycle and Greenhouse Gases Group Continuous Insitu Measurements of CO2 at Global
1042 Background Sites, 1973-Present, https://doi.org/10.15138/YAF1-BK21, 2023.

1043 Tzortziou, M., Neale, P. J., Osburn, C. L., Megonigal, J. P., Maie, N., and JaffÉ, R.: Tidal
1044 marshes as a source of optically and chemically distinctive colored dissolved organic matter in
1045 the Chesapeake Bay, Limnology and Oceanography, 53, 148–159,
1046 https://doi.org/10.4319/lo.2008.53.1.0148, 2008.

1047 Tzortziou, M., Neale, P. J., Megonigal, J. P., Pow, C. L., and Butterworth, M.: Spatial gradients
1048 in dissolved carbon due to tidal marsh outwelling into a Chesapeake Bay estuary, Marine
1049 Ecology Progress Series, 426, 41–56, https://doi.org/10.3354/meps09017, 2011.

1050 Unsworth, R. K. F., Cullen-Unsworth, L. C., Jones, B. L. H., and Lilley, R. J.: The planetary role
1051 of seagrass conservation, Science, 377, 609–613, https://doi.org/10.1126/science.abq6923, 2022.

1052 Upstill-Goddard, R. C.: Air–sea gas exchange in the coastal zone, Estuarine, Coastal and Shelf
1053 Science, 70, 388–404, https://doi.org/10.1016/j.ecss.2006.05.043, 2006.

1054 Van Dam, B. R., Edson, J. B., and Tobias, C.: Parameterizing Air-Water Gas Exchange in the
1055 Shallow, Microtidal New River Estuary, Journal of Geophysical Research: Biogeosciences, 124,
1056 2351–2363, https://doi.org/10.1029/2018JG004908, 2019.

1057 Wanninkhof, R.: Relationship between wind speed and gas exchange over the ocean, Journal of
1058 Geophysical Research: Oceans, 97, 7373–7382, 1992.

1059 Wanninkhof, R.: Relationship between wind speed and gas exchange over the ocean revisited,
1060 Limnology and Oceanography: Methods, 12, 351–362, https://doi.org/10.4319/lom.2014.12.351,
1061 2014.

1062 Wanninkhof, R. and McGillis, W. R.: A cubic relationship between air-sea CO2 exchange and
1063 wind speed, Geophysical Research Letters, 26, 1889–1892,
1064 https://doi.org/10.1029/1999GL900363, 1999.

1065 Wanninkhof, R., Park, G.-H., Takahashi, T., Sweeney, C., Feely, R., Nojiri, Y., Gruber, N.,
1066 Doney, S. C., McKinley, G. A., Lenton, A., Le Quéré, C., Heinze, C., Schwinger, J., Graven, H.,

and Khatiwala, S.: Global ocean carbon uptake: magnitude, variability and trends, Biogeosciences, 10, 1983–2000, https://doi.org/10.5194/bg-10-1983-2013, 2013.

Waycott, M., Duarte, C. M., Carruthers, T. J. B., Orth, R. J., Dennison, W. C., Olyarnik, S., Calladine, A., Fourqurean, J. W., Heck, K. L., Hughes, A. R., Kendrick, G. A., Kenworthy, W. J., Short, F. T., and Williams, S. L.: Accelerating loss of seagrasses across the globe threatens coastal ecosystems, Proceedings of the National Academy of Sciences, 106, 12377–12381, https://doi.org/10.1073/pnas.0905620106, 2009.

Weiss, R. and Price, B.: Nitrous oxide solubility in water and seawater, Marine Chemistry, 8, 347–359, https://doi.org/10.1016/0304-4203(80)90024-9, 1980.

Winslow, L. A., Zwart, J. A., Batt, R. D., Dugan, H. A., Woolway, R. I., Corman, J. R., and Read, J. S.: LakeMetabolizer: An R package for estimating lake metabolism from free-water oxygen using diverse statistical models, Inland Waters, 6, https://doi.org/10.1080/IW-6.4.883, 2016.

Xiao, S., Liu, L., Wang, W., Lorke, A., Woodhouse, J., and Grossart, H.-P.: A Fast-Response Automated Gas Equilibrator (FaRAGE) for continuous in situ measurement of CH_4 and CO_2 dissolved in water, Hydrology and Earth System Sciences, 24, 3871–3880, https://doi.org/10.5194/hess-24-3871-2020, 2020.

Zeebe, R. E. and Wolf-Gladrow, D.: CO2 in Seawater: Equilibrium, Kinetics, Isotopes, Gulf Professional Publishing, 382 pp., 2001.

Supplemental

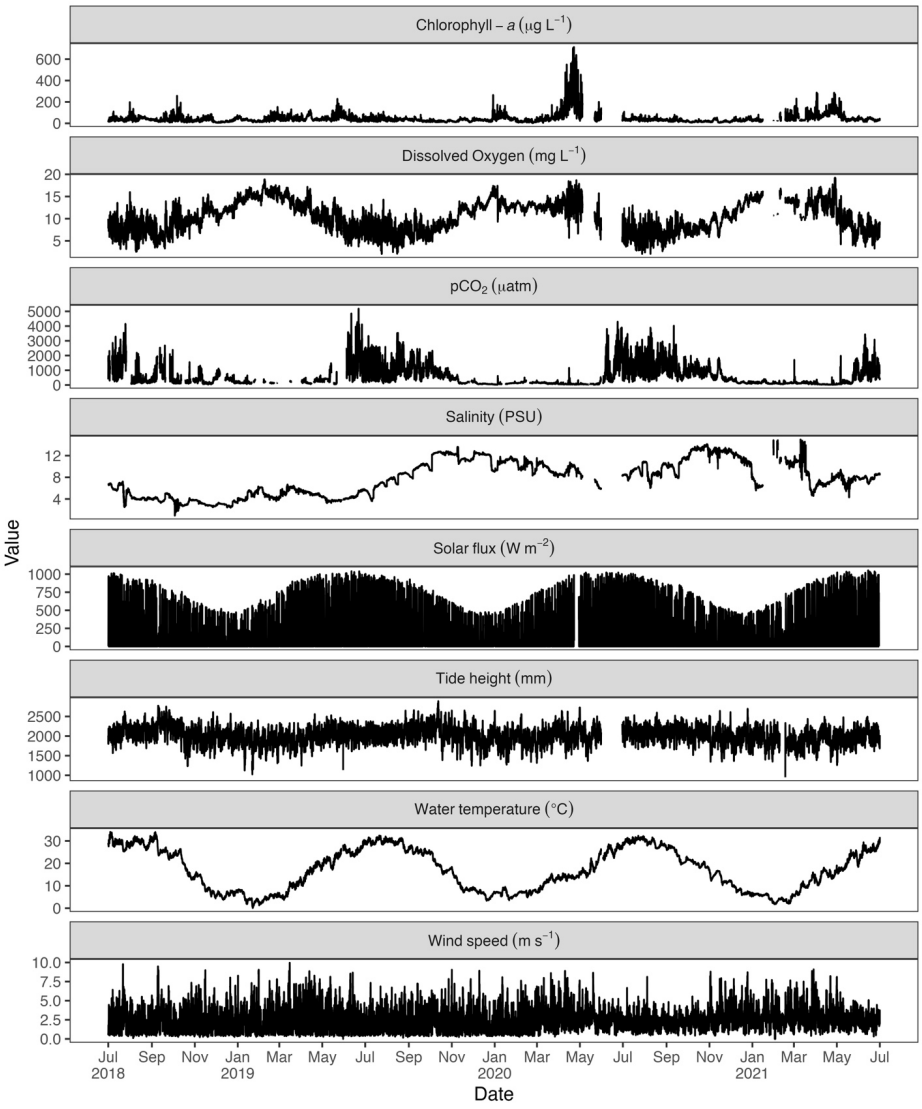

Fig. S1. Plot of all raw values from environmental variables for the same time period as CO_2 flux (July 2018–July 2021).

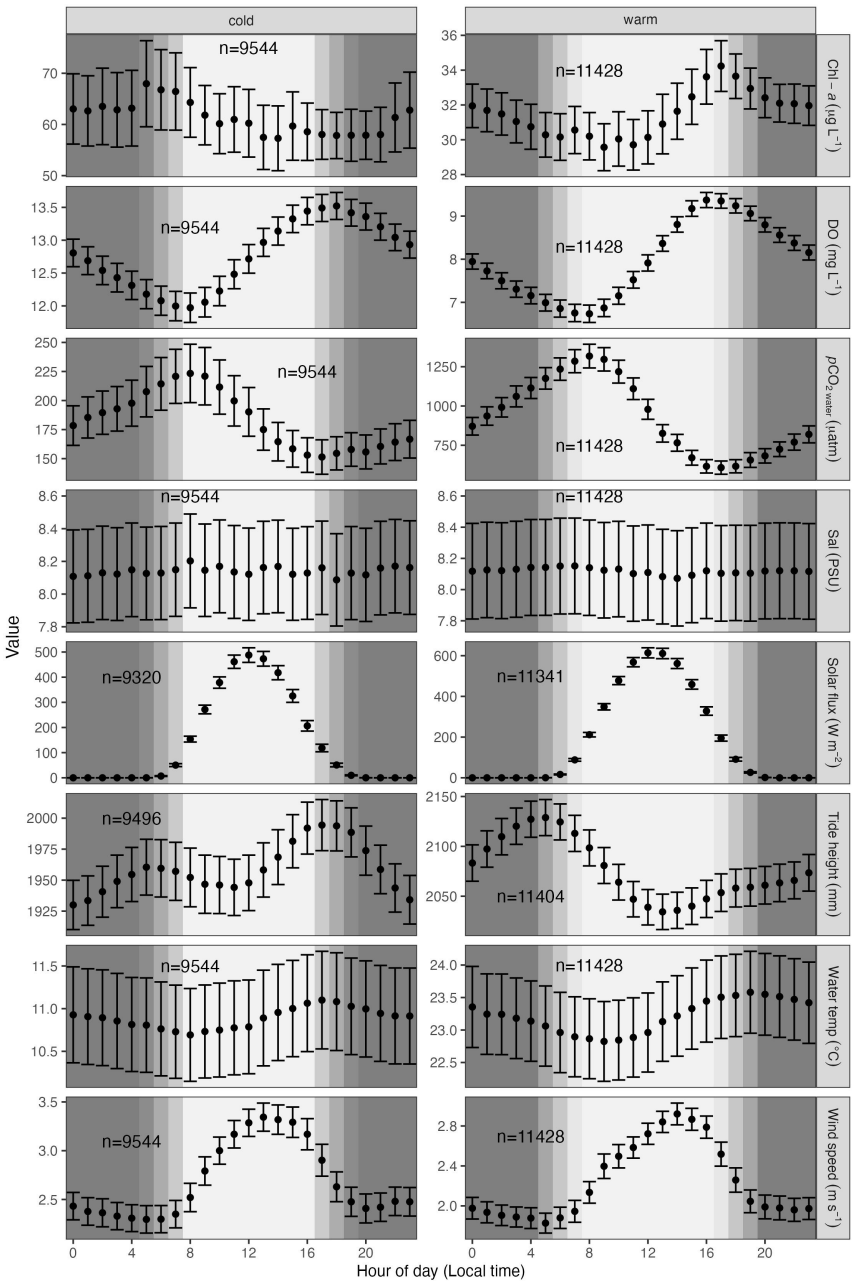
cold
warm
n=9544
n=11428
n=9320
n=11341
n=9496
n=11404
Chl – a (µg L⁻¹)
DO (mg L⁻¹)
pCO2 water (µatm)
Sal (PSU)
Solar flux (W m⁻²)
Tide height (mm)
Water temp (°C)
Wind speed (m s⁻¹)
Value
Hour of day (Local time)

Fig. S2. Average hourly values (95% CI) of environmental variables across 24 hours of the day (July 2018–July 2021) in cold and warm seasons. Light/dark background indicates day/night conditions.

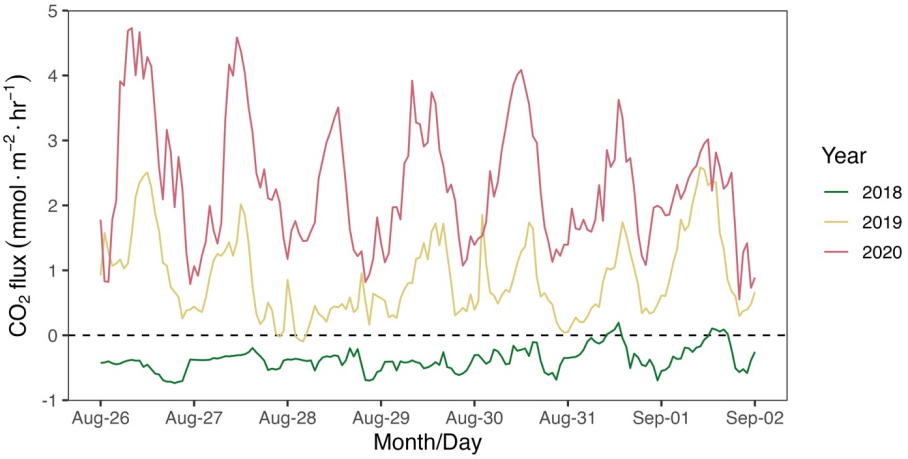

Fig. S3. Hourly CO_2 flux estimates for the week of August 26 to September 2 where CO_2 flux status differs among years.

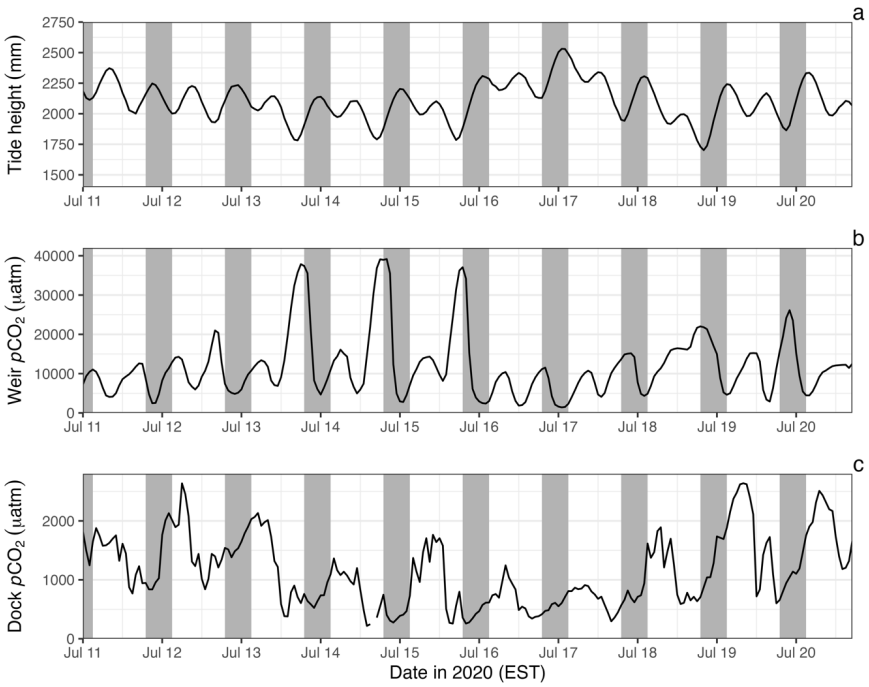

Fig. S4. Simultaneous pCO_2 measurements (1 hr intervals) from SERC dock (panel c) and the mouth of the single tidal creek that drains the Kirkpatrick Marsh (panel b) (11–20 Jul 2020) indicate that dissolved CO_2 varies at the dock according to a day/night cycle while CO_2 in the marsh tidal creek rises and falls inversely with tide height (panel a), indicating outwelling of marsh derived CO_2 (e.g., root respiration, pore and groundwater).